Cladding thickness of fuel elements by X-rays

Lowe, Beverly James.; Sierer, Payson Dwight.

Massachusetts Institute of Technology

CLADDING THICKNESS OF FUEL ELEMENTS BY X-RAYS

BEVERLEY JAMES LOWE
AND
PAYSON DWIGHT SIERER, JR.

CLADDING THICKNESS OF FUEL ELEMENTS BY X-RAYS

by

BEVERLEY JAMES LOWE

and

PAYSON DWIGHT SIERER JR.

SUBMITTED IN PARTIAL FULFILLMENT OF THE REQUIREMENTS FOR THE DEGREE OF NAVAL ENGINEER AND THE DEGREE OF MASTER OF SCIENCE IN NAVAL ARCHITECTURE AND MARINE ENGINEERING

at the

MASSACHUSETTS INSTITUTE OF TECHNOLOGY

May 1958

Signature of Authors _____

_____

Massachusetts Institute of Technology
May 26, 1958

Certified by _____
Thesis Supervisor

Accepted by _____
Chairman, Departmental Committee on
Graduate Students

CLADDING THICKNESS OF FUEL ELEMENTS BY X-RAYS

by

BEVERLEY JAMES LOWE

and

PAYSON DWIGHT SIERER JR.

Submitted to the Department of Naval Architecture and Marine Engineering on May 26, 1958 in partial fulfillment of the requirements for the degree of Naval Engineer and the degree of Master of Science in Naval Architecture and Marine Engineering.

ABSTRACT

This thesis investigates the feasibility of non-destructive testing techniques for the determination of cladding thickness on uranium fuel elements. The techniques investigated were uranium X-ray fluorescence attenuation and Compton scattering of photons from the cladding surface. Both spectroscopic and non-dispersive analysis techniques were employed in the investigation.

The use of both the L and the K characteristic X-ray series of uranium was investigated for the various cladding materials. The investigation of the Compton scattering technique was also divided into two phases, based on the source of the photons. The first employed low energy photons from an industrial X-ray unit, the second employed the

radiation from a radium source.

The results of the investigation have shown that the thickness of cladding on uranium fuel elements can be successfully measured, with accuracies up to one percent, by the use of the proposed techniques. The particular technique employed is a function of the atomic number and density of the cladding material.

Thesis Supervisor: Robert E. Ogilvie

Title: Assistant Professor of Metallurgy

ACKNOWLEDGEMENTS

The authors would like to acknowledge their obligations to those who have aided in the preparation of this thesis: to the MIT Metallurgy Department and to Sheldon H.Moll for the generous loan of equipment; to Nuclear Metals, Inc. for the provision of sample uranium fuel specimens. The authors are particularly indebted to our thesis advisor, Robert E. Ogilvie, at whose suggestion this thesis was initiated. His assistance and advice has been of invaluable aid. Above all this we owe a special debt of thanks to our respective wives whose limitless patience and encouragement has made it possible for this work to be completed.

B. J. Lowe

P. D. Sierer Jr.

TABLE OF CONTENTS

LIST OF TABLES

LIST OF TABLES

LIST OF TABLES

LIST OF FIGURES

LIST OF FIGURES

INTRODUCTION

The purpose of the thesis was to investigate, and evaluate as a production process, non-destructive testing techniques for the determination of metallic cladding thicknesses on uranium fuel elements. The techniques investigated were X-ray fluorescence and Compton scattering, employing both spectroscopic and non-dispersive techniques as described under the respective sections on procedure.

Cladding on reactor fuel elements is necessary because of the reactive characteristics of uranium metal. Uranium, in both its solid and liquid form, readily forms chemical bonds with water, the atmosphere and a large variety of organic and inorganic materials. Because of these chemical characteristics of uranium the reactor industry has devoted considerable energy and expense in providing protective metal coatings to the reactor fuel elements. At the present time, application of this protective coating is usually accomplished by either electroplating, "canning" or co-extrusion processes, with the latter being preferred because of the required thickness of the cladding material and economic considerations. Because of the irreversible corrosion effects and damages that could occur should the cladding material be outside of acceptable tolerances, it is desirable that some reliable method of quality control be employed to insure proper performance during reactor operation.

The present non-destructive testing techniques now in use or under investigation are: 1- autoradiographic techniques employing the natural 0.18 Mev Gamma ray of uranium, and 2- attenuation measurements of the 2.3 Mev Beta ray emitted by the Pa^{234} daughter of U^{238} [7] . Sufficient information on the techniques to properly evaluate them was not given by the author, however, the autoradiographic technique is extremely slow (8-16 hours for a typical exposure) and therefore not well suited for a production process. The Beta ray attenuation process appears to be promising, but sufficient information to properly evaluate the technique was not presented.

A literature survey failed to reveal any previous investigation of the applicability of the proposed techniques to non-destructive testing of reactor fuel elements. The technique of X-ray fluorescence has been applied to the determination of thin plating thicknesses, and has been industrially applied for the determination of thickness of tin plating on steel.[1] However, no references were found indicating industrial application of this technique for testing of cladding thicknesses of the order used in cladding uranium fuel elements.

Application of the photon scattering and absorption phenomenon to industrial uses other than X-ray or Gamma ray photographic or chemical analysis techniques has few references in the literature. One reference[12] notes that gamma scattering has been successfully employed in

determining the density or thickness of materials. It is also known that gamma ray densitometers are being employed in the petroleum industry to determine the density of various mixtures being transmitted through piping conduits. No references to the latter procedures could be found. In no case were any references found which indicated or suggested that photon scattering be employed as a means of determining the thickness of a cladding material on a base metal.

This dearth of literature in relation to the proposed techniques could be reasonably expected in that the success of the proposed techniques is dependent upon large differences in atomic number between the base material and the cladding material. This criterion is particularly well met in uranium fuel rods, where the physical, chemical, and thermal characteristics of the reactor dictate that the cladding material be one of the lighter elements. Inasmuch as the base metal is uranium, which is at the upper end of the atomic scale, the situation for the proposed techniques is optimized. Relatively older industries would normally have no possible application of the techniques since industrial metallurgy has been generally restricted to elements of lower atomic number.

Essentially the proposed techniques for the determination of cladding thickness on uranium fuel rods are based on two different interactions of photons with matter. These interactions of photons with matter which are of importance to the thesis are: 1-the ejection of a K or L

electron from the atom by the incident photon, with the resultant production of the K or L series of fluorescent radiation, and 2- the elastic scattering of the incident photon by the atomic electrons. The predominance of one type of interaction over the other is a function of the atomic number of the target material and the energy of the incident photon. As the energy of the incident photon is increased to much higher levels a third type of interaction, not applicable to the thesis, occurs. This is the pair production effect which occurs above the threshold energy of 1.02 Mev. Figure I shows diagrammatically the regions of predominance of the various interactions in terms of atomic number and incident photon energy.

The proposed method of cladding thickness determination by X-ray fluorescence depends upon the correlation between the attentuation of the fluorescence X-ray beam by the cladding material and the thickness of the cladding material. The relation between attentuation of the X-ray beam and the thickness of material is given by the expression:

$$I_x = I_o e^{-\mu x} \qquad (1)$$

where I_o is the initial intensity of the incident X-ray beam, I_x is the intensity of the beam after traversing a distance x of the absorber and μ is the linear attenuation coefficient of the material.

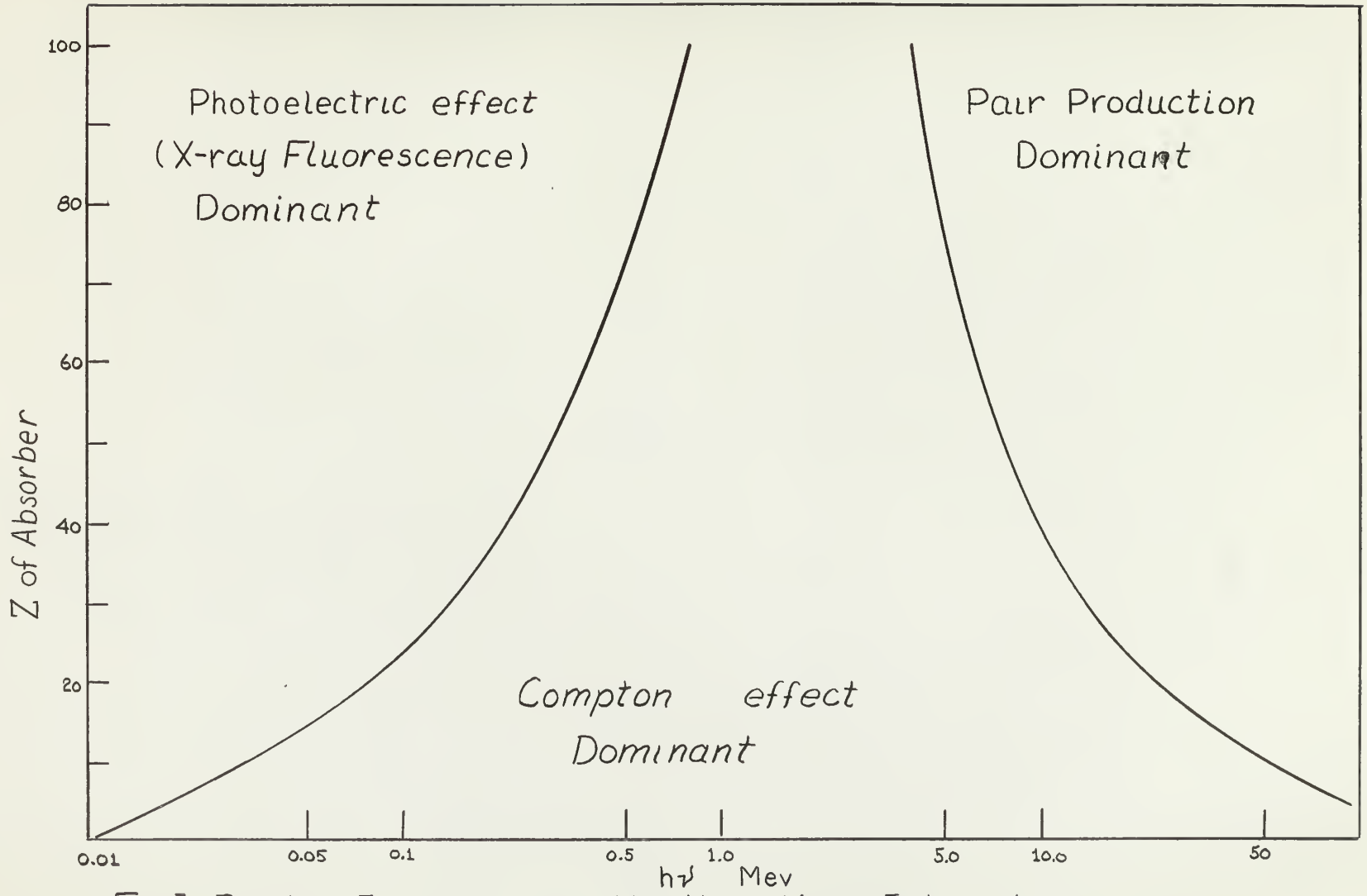

Figure I

FIG I Relative Importance of the three Major Interactions
from The Atomic Nucleus R. D. Evans

As seen from Figure I the most predominant interaction at the photon energy under consideration is the true absorption interaction wherein the photon ejects an atomic electron resulting in the emission of characteristic X-ray spectra. (Also known as the photo-electric effect.) Since the linear attenuation coefficient is the sum of the scattering and absorption coefficients the behavior of the linear coefficient with atomic number and energy will follow the behavior of the most predominant interaction, that of absorption.

A rough, empirical relation indicating the dependence of the true absorption coefficient on photon energy and the atomic number of the absorber is given by: [5]

$$\tau \approx \text{const} \quad \frac{Z^4}{(h\nu)^3} \qquad (2)$$

where $h\nu$ is the energy of the photon, Z is the atomic number of the absorber and τ is the absorption coefficient. Since density is proportional to Z and the energy, $h\nu$, is inversely proportional to the wavelength of a photon, the above relationship agrees with the empirical relationship used in the field of X-ray diffraction:

$$\frac{u}{\rho} = k \lambda^3 Z^3 \qquad (3)$$

where $\frac{u}{\rho}$ is the mass absorption coefficient, k is an empirically determined constant and λ is the wavelength of the incident photon.

The above relationship indicates that the total attenuation coefficient of a material increases with increasing atomic number and density, and decreases with increasing photon energy. The effect of this dependence on the measurement of cladding thickness will be further discussed under procedure.

SECTION A

X-RAY FLUORESCENT INVESTIGATION

SECTION A

X-RAY FLUORESCENCE THEORY

The phenomenon of X-ray fluorescence, or characteristic X-ray emission, occurs whenever any process results in the removal of K , L , or higher shell electrons, creating an electron vacancy in these shells. The process employed in this thesis was the removal of a K or L shell electron by a collision with an X-ray photon of sufficient energy to overcome the binding energy of the atomic electron and eject it from the atom. Other processes which could result in X-ray fluorescence are collision of the atomic electron with an energetic free electron or an electron capture nuclear transition. The removal of the atomic electron leaves the atom in an ionized state, and the ensuing rearrangement of atomic electrons as the atom proceeds to a lower energy level results in the emission of one or more X-ray quanta of energy, Auger electrons, or both, depending upon the atomic number of the atom. Since the thesis is concerned only with X-ray fluorescence, and since uranium, with an atomic number of 92 has a fluorescence yield of almost unity, the Auger electrons will not be discussed. [5]

X-ray fluorescence was first noted as early as 1896 by Winkelmann and Straubel in X-ray experiments with Fluor Spar, however, they concluded at the time that it was caused by some type of reflective mechanism. It remained

for Barkla and his collaborators, in 1906, to determine that this secondary radiation was actually emitted from the target, and that this fluorescent radiation was characteristic of the target material. Considerable work was done in the field of characteristic X-ray radiation by Laue, Bragg, and Moseley. Moseley, although unable to explain the mechanism of production of characteristic X-ray spectra, was able to construct an empirical relationship between the frequency of the characteristic X-ray line and the atomic number of the emitter. It was about this time, 1913, that Bohr introduced his quantum theory of the origin of atomic spectra, which gave a theoretical explanation for the phenomenon of X-ray fluorescence.

According to Bohr's theory the energy, $h\nu$, of characteristic X-ray quanta would be given by the relationship:

$$h\nu = Z^2 \frac{2\pi^2 m_o e^4}{h^2} \left[\frac{1}{n_1^2} - \frac{1}{n_2^2} \right] \qquad (4)$$

where n_1 and n_2 are the principal quantum numbers for the initial and final electron vacancies, Z is the atomic number of the nucleus, h is Planck's constant, e the charge on the electron and m_o the mass of the electron.

The empirical relationship between ν and Z established by Moseley for the K_α series of characteristic X-rays can be expressed as:

$$\nu = 0.248 \times 10^{16} (Z-1)^2 \qquad (5)$$

If the values of $n_1 = 1$ and $n_2 = 2$ (the principal quantum numbers for the initial and final electron vacancy for the K_α series) are inserted in Equation (1) we obtain:

$$\nu = 0.246 \times 10^{16} Z^2 \qquad (6)$$

This close agreement between theory and experiment indicated that the hypothesis of an electron vacancy being filled by the transition of an electron in one quantum state to a lower quantum state with the accompanying emission of a quantum of energy was correct. According to Bohr's theory, Equation (1), the quantum of energy emitted was proportional to the charge on the nucleus, however, for all atoms but hydrogen there are two electrons corresponding to the principal quantum number $n = 1$. For atoms of higher atomic number there are up to eight electrons in quantum states with $n = 2$ (L electrons), and if Z is high enough there will be M electrons ($n = 3$) extending still farther out from the nucleus, and so on. For any particular transition from one quantum state to another the effective nuclear charge will be somewhat less than Ze due to the shielding

of the nuclear charge by the potential due to the K , L ,... electrons present between the nucleus and the electron undergoing the transition. This hypothesis explains, qualitatively at least, the discrepancies between Bohr's theory and Moseley's empirical relationship. Moseley's screening constants of unity for the K_α series and 7.4 for the L_α series are physically reasonable in the light of this hypothesis. Further work in the field of characteristic spectra, however, has shown that the quantitative results of Moseley's Law holds only as a first approximation.

As soon as equipment of high enough resolving power was available, it was found that a fine structure existed in the characteristic X-ray spectra indicating the existence of multiplet energy levels within the principal quantum states. For a satisfactory explanation of this fine structure, it is necessary to turn to the more complex concepts of orbital angular momentum and spin-orbit interaction effects contained in wave mechanics.

In the derivation of his theory Bohr made the assumption that the electron revolves around the nucleus in a circular orbit with the angular momentum of the electron equal to $n \frac{h}{2\pi}$, or $\ell = n$, where ℓ is the number of units of quantized angular momentum assigned to the atomic electron. This leads to the conclusion that there is a single energy level for each principal quantum level.

This conclusion is not consistent with the fine structure noted in characteristic X-ray spectra, indicating several different L , M ,... levels lying close together.

In contrast to the results of the Bohr theory the application of wave mechanics to the problem of a central field approximation for a many-electron atom [9] indicates that electronic states are characterized by four quantum numbers, n , ℓ , λ and μ , which are subject to the restriction that n , ℓ and λ are integers or zero, and:

$$n > \ell \geq |\lambda| \qquad \mu = \pm \tfrac{1}{2}$$

For convenience in designating electronic quantum states the value of ℓ may be represented by letters as follows:

ℓ	0	1	2	3	4	5	6
	s	p	d	f	g	h	i

The energy of an electron in the modified central field depends, as in the Bohr theory, mainly upon the principal quantum number, n , but in this case it now also varies slightly with ℓ , decreasing in magnitude with increasing ℓ . The quantum configuration of the lowest electronic energy state (corresponding to the K , $n = 1$, shell of the Bohr model) is the 1s state ($n = 1$, $\ell = 0$, $\mu = \pm \frac{1}{2}$).

The next lowest states are the 2s states ($n = 2$, $\ell = 0$, $\lambda = 0$, $\mu = \pm \frac{1}{2}$). The six 2p states ($n = 2$, $\ell = 1$, $\lambda = 1, 0, -1$ and $\mu = \pm \frac{1}{2}$) lie just above the 2s states in energy level.

The final step in the development of the theory to explain multiplet levels in electronic quantum states was the consideration of the spin-orbit interaction effect in a central field model. [9] In this case the relativistic interaction between the magnetic moment of the classically "spinning" electron and the spherically symmetrical electric field modifies the solution so that the electronic quantum states are described by the quantum numbers n, ℓ, j and m, where n is the principal quantum number, ℓ is the orbital angular momentum expressed in units of $\frac{h}{2\pi}$, and j represents, in units of $\frac{h}{2\pi}$, the maximum numerical value of the axial component of the vector sum of the orbital angular momentum and the spin of the atomic electron. The quantum number m represents integrally spaced values of the projection of the j vector on the chosen axis. The allowable values for the quantum numbers, n, ℓ, j, m, with the quantum number corresponding to electron spin, s, equal to $\pm \frac{1}{2}$, become:

$$n > \ell \quad ; \quad j = \ell + s = \ell + \tfrac{1}{2}$$

$$j \geq m \geq -j \text{ (integrally spaced)}$$

When spin-orbit interaction is considered the energy depends on j as well as n and ℓ, and each $n\ell$ energy level, with $\ell > 0$ is split into two sub-levels. A further result of the wave mechanic solution is that all transitions between quantized energy levels are no longer possible. The allowed transitions are those which $\triangle \ell = \pm 1$ and $\triangle j = \pm 1,0$.

The theory outlined in the preceding paragraphs indicates that for each $n\ell$ quantum level with $\ell > 0$ the spin-orbit interaction results in the formation of two sub-levels. Thus, for the K level there would be only one energy level ($n = 1$, $\ell = 0$, $j = \frac{1}{2}$), for the L level, however, there would be three levels: L_I ($n = 2$, $\ell = 0$, $j = \frac{1}{2}$), L_{II} ($n = 2$, $\ell = 1$, $j = \frac{1}{2}$) and L_{III} ($n = 2$, $\ell = 1$, $j = 3/2$). This result, in conjunction with the selection rules previously given, predict two allowed transitions between electrons in the L shell and vacancies in the K shell. These transitions are from the L_{II} level to the K level, and from the L_{III} to the K level. These theoretical results correlate with experimental observations, the L_{II} transition corresponding to the K_{α_2} spectral line, the L_{III} transition corresponding to the K_{α_1} spectral line.

Figure II illustrates the energy levels for uranium and shows all allowable transitions permitted by the selection rules. The various spectral lines are indicated by their series and sub-level.

Figure II

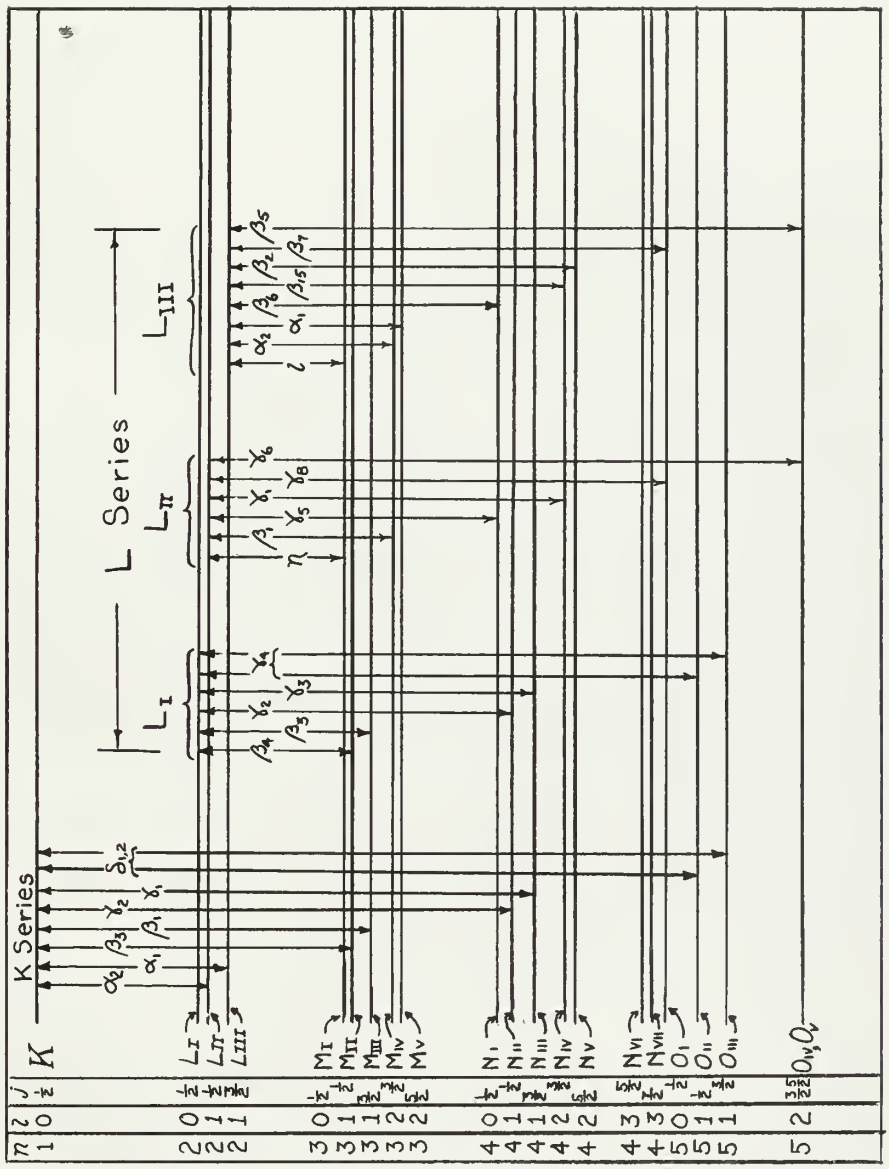

Fig. II. X-ray Energy Level Diagram for Uranium
from Intro. to Modern Physics
Richtmyer, Kennard and Lauritsen

PROCEDURE

In determining the thickness of cladding material on uranium fuel elements it was proposed to excite the characteristic X-ray spectrum of uranium by means of an external X-ray source, and then determine the attenuation of the characteristic X-ray in passing through the cladding material. The wide range encountered in the atomic number and density of cladding materials precluded using any one characteristic series of uranium to successfully measure all cladding materials. Fortunately, the atomic number of uranium is high enough that both the K and L characteristic X-ray series are of a high enough energy level to be used in fluorescent analysis. The cladding materials of high atomic number which are virtually opaque to the L series of uranium have reasonable attenuation coefficients for the higher energy K series, while the low atomic number, low density cladding materials, which are virtually transparent to the K fluorescent series of uranium have appreciable attenuation coefficients at the energy of the uranium L fluorescent series.

In exciting the characteristic X-ray series of clad uranium the characteristic X-ray series of the cladding material is also excited. Since excitation energy increases as a function of atomic number, and the cladding material will be of lower atomic number than the fuel material this excitation of the cladding fluorescent series cannot be

avoided. As a result the radiation reaching the detector from the fuel rod will be polychromatic in nature and contain: 1-the characteristic uranium series, 2-the characteristic cladding series and 3-a brehmstralung of scattered radiation. In order to analyze this polychromatic beam in terms of cladding thickness, it is necessary to determine the intensity distribution of the spectrum as a function of energy, or in effect to separate the uranium fluorescent series from the remainder of the spectrum. This can be done by means of a crystal spectrometer or a pulse height analyzer. In cladding materials of low atomic number, such as aluminum, the characteristic X-ray series is of such low energy that the air path from the specimen to the detector effectively filters out all aluminum fluorescence. For this situation it would be possible to employ a non-dispersive technique and eliminate the need for an analyzing device. In all phases of this investigation, however, the authors employed an analyzing device. For L fluorescence investigations a lithium fluoride crystal spectrometer was used, and all analysis was performed employing the intensity of the L_{α_1} line. In the K fluorescence investigation a pulse height analyzer was employed due to the difficulty involved in obtaining and orienting a crystal with sufficiently small interplanar spacing.

The investigation was essentially a feasibility study for the various techniques involved, and the equipment used was originally designed with entirely different applications

in mind. For this reason many of the experiments had to be designed around the limitations of the equipment and were not carried out in the optimum geometry for cladding thickness determination.

Uranium L Series Fluorescent Technique:

A commercially available Norelco X-ray Fluorescent Analysis unit was used to determine the feasibility of cladding thickness measurement utilizing the uranium L series fluorescence. The exciting X-ray source was equipped with an electronic voltage and current stabilizer, which, when operated between designed limits, maintained tube input current to within $\pm$ 0.1% of the assigned value.

The detecting device used in conjunction with the fluorescent analysis unit was a scintillation detector driving a scaler through a linear amplifier. (See Appendix A for details of the equipment.)

Due to the restriction imposed by the specimen holder of the fluorescent analysis unit, fuel elements had to be simulated by a flat slab approximation. A flat disc of natural uranium, covered by cladding material foils of known thickness, was used to simulate a fuel element. The flat plate approximation is perfectly satisfactory for a feasibility study, and lends itself readily to theoretical analysis.

The three cladding materials chosen for investigation were aluminum, stainless steel and zirconium. These

materials represent a rather wide range of atomic number, and are in common use as cladding materials. The characteristic uranium L series line that was employed throughout the experiment was the L_{α_1} line, since this provided the highest intensity, and hence the lowest statistical error in the results. All recorded data was taken by the "fixed count" method to maintain a constant statistical error.

The procedure involved in determining a calibrated curve of fluorescent counting rate vs. cladding thickness was straightforward and consisted of taking a series of "fixed count" measurements of the intensity of the uranium L_{α_1} spectral line for various known thicknesses of cladding material. For aluminum, a total of 102,400 counts was recorded for each cladding thickness, reducing the standard deviation of the mean counting rate to 0.31%. For other cladding materials the initial results obtained for L series fluorescence did not warrant the high level of statistical accuracy. This is indicated in the data shown for stainless steel and zirconium studies.

The maximum thickness of any one cladding material that could be successfully measured by L series fluorescence was a function of geometry and the intensity and energy of the exciting X-ray source. The geometry controls the effective thickness of cladding presented to the incident and fluorescent X-ray beam, while the intensity and energy of the exciting X-ray source controls the fluorescent intensity and hence the cladding thickness at

which the fluorescent intensity is reduced to background intensity. Unfortunately, both the geometry and the maximum permissible fluorescent intensity were fixed by considerations of the equipment in use. The geometry was fixed by the relation between the specimen holder and the analyzing crystal, while the initial fluorescent intensity was limited to approximately 1300 counts per second due to the mechanical limitations of the counting register.

For aluminum, the above restrictions limited the procedure to a cladding thickness of approximately 10 mils if reasonable accuracy in measurement was to be maintained. This procedural difficulty was overcome by using a cladding thickness of 20 mils as the initial point, and increasing the energy and intensity of the incident X-ray beam until the intensity of the uranium L_{α_1} line approached the upper limit allowed by the mechanical register. By basing the initial L_{α_1} intensity on 20 mils of aluminum cladding the relationship between cladding thickness and L_{α_1} intensity could be determined from 20 to 30 mils of cladding with good accuracy.

The energy of the exciting X-ray source for L fluorescence investigations was varied to suit requirements for initial counting rates. The lower limit for the exciting X-ray source was the energy required to remove an L shell electron from the uranium atom. Excitation energies for the materials used in the investigation are listed in Appendix C.

Uranium K Series Fluorescent Technique

In determining the feasibility of cladding thickness measurement by use of the uranium K series fluorescence, a 150 kev - 8ma commercially available X-ray unit was used as a radiation source. The X-ray source was used in conjunction with a voltage stabilizer.

The detection and recording equipment used in this phase of the investigation was identical to that used for the uranium L series investigation. Spectrum analysis was accomplished by the use of a pulse height analyzer as opposed to the lithium fluoride crystal used in the uranium L series tests. (See Appendix B for details of the equipment.)

The X-ray beam was collimated by means of a long lead cylinder. Both the X-ray unit and the detection equipment were thoroughly shielded to reduce the scattered radiation. (See Figure XX for sketch of geometry of experiment.) This shielding was entirely adequate in that background readings taken without the specimens in place were so low as to be considered insignificant.

The cladding materials chosen for investigation were stainless steel (304) and zirconium. An analysis was not conducted on aluminum for two reasons: 1-Successful correlation had already been obtained utilizing the uranium L series, and 2-The atomic number of aluminum was sufficiently low that the attenuation and scattering characteristics of aluminum were expected to be formidable difficulties. High scattering would prove troublesome in that the attenua-

Fig. III Tubular Fuel Element Specimen

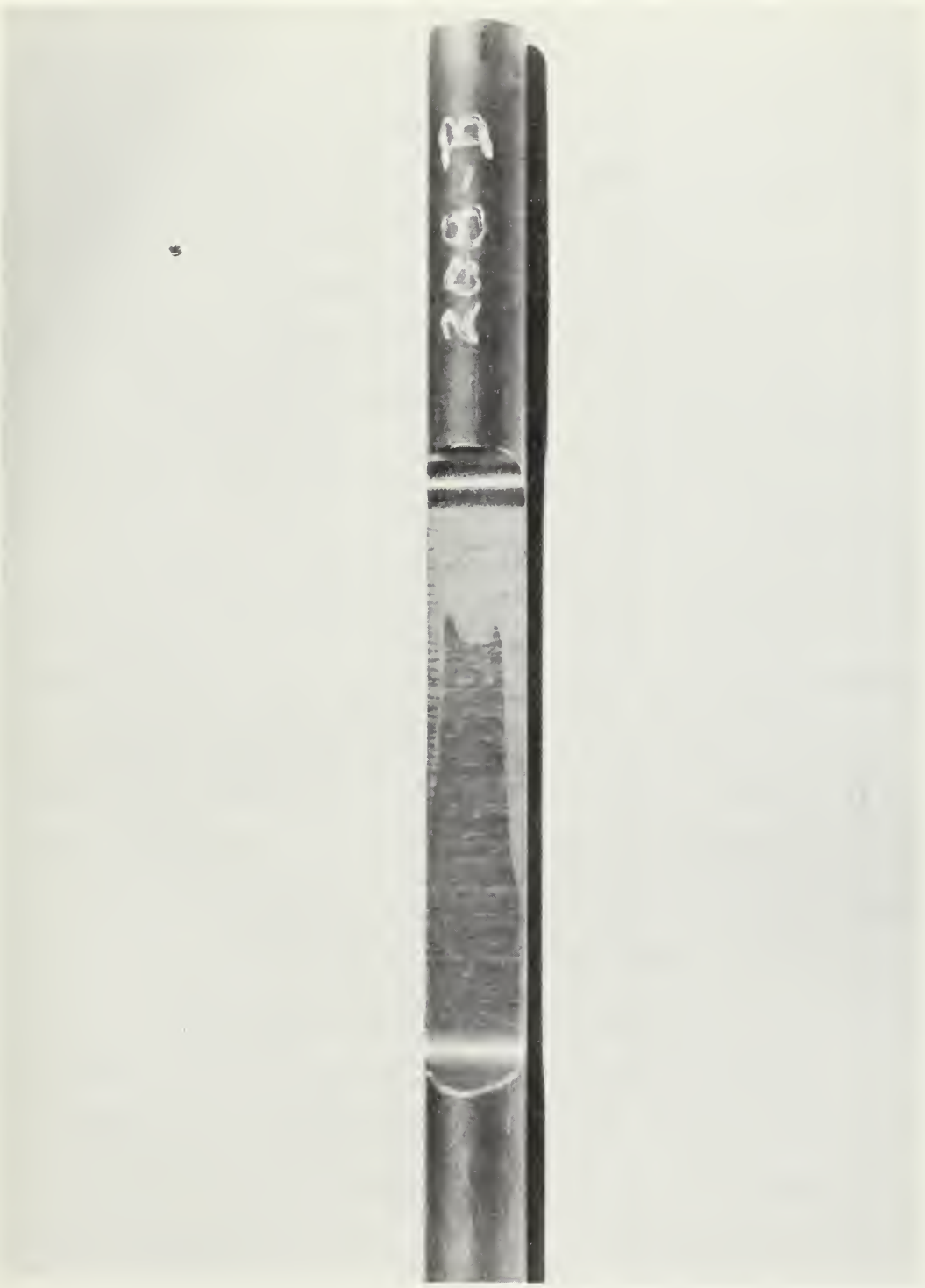

Fig. IV Sectioned Cylindrical Fuel Element

tion of the fluorescent radiation would be more than compensated by the increase in scattered radiation. As is indicated in subsequent development, these predictions were confirmed in that excessive scattering also prevented successful correlation of uranium K series fluorescence with the cladding thickness of stainless steel.

Uranium clad elements were simulated by flat plate approximations for an initial feasibility study. To further demonstrate the applicability of the technique to industrial applications, two scanning runs were made of typical uranium fuel elements. Both of these fuel elements (Figures III and IV) were clad with Zircalloy-II; one with cladding thickness of the order of approximately 5 to 10 mils, the other of approximately 40 mils. The tubular fuel element (Figure III) had been measured accurately by visual means by Nuclear Metals, Inc., of Cambridge, Massachusetts. This latter element provided a reasonable standard of comparison and both fixed and scanning runs were conducted on it. Unfortunately, the scribe location indicating the relative origin for the visual data compiled by Nuclear Metals, Inc. could not be identified and apparent correlation could only be indicated by means of the symmetry of the two plots. A longitudinal scan was also conducted on a sectioned fuel element (Figure IV).

The determination of a calibrated curve of fluorescent radiation intensity vs. cladding thickness utilizing a non-dispersive technique required an initial analysis of the

energy spectrum in order to optimize operating conditions. Preliminary scanning runs of the uranium and the cladding materials indicated maximum resolution of the uranium K series fluorescence peak and the cladding scattering peak at a dynode voltage of 900 volts. This optimum dynode voltage was determined by making scans of the energy spectrum for uranium and the cladding materials and determining resolution as a function of dynode voltage. With the optimum dynode voltage established, additional scans of the spectrum were made to insure accurate determination of a suitable operating point for the pulse height analyser (base line voltage and window width) to insure operation of counting runs at the uranium K series fluorescence peak. (Figure XIX (a) through (f) indicate typical curves of energy spectrum intensity vs. pulse height analyser base line voltage.)

When the fluorescent peak of the uranium was determined as outlined above and the pulse height analyzer operating point established, a series of "fixed count" measurements of the intensity of fluorescent radiation for various known thicknesses of the cladding material were made. For zirconium and stainless steel, a total of 25,600 counts were recorded for each cladding thickness, reducing the standard deviation of the mean counting rate to 0.62 per cent.

In conducting "fixed count" measurements of the tubular fuel element (Figure III) a series of seven 25,600 count

measurements were conducted at intervals of 10 degrees around the specimen. These exhaustive measurements were made to reduce the effects of instabilities in the operating equipment. Following completion of the "fixed count" runs, a rotational scan at the rate of one revolution per minute was made with results recorded on a Brown recorder. (See Figure IX .)

The results of the longitudinal scan conducted on the sectioned cylindrical element were also recorded on a Brown recorder. (See Figure X .)

RESULTS

L FLUORESCENCE INVESTIGATION

TABLE I

NORMALIZED URANIUM L FLUORESCENT INTENSITY

Vs.

ALUMINUM CLADDING THICKNESS

Background and Scattering Included

Cladding thickness (mils)	I
20	1.000
21.8	0.787
23.6	0.651
25.4	0.526
26.7	0.412
28.5	0.351
30.0	0.281
31.8	0.250
33.5	0.221
33.6	0.222
35.4	0.200
36.7	0.178
40.0	0.150
43.6	0.145
45.4	0.139
50.4	0.132
60.9	0.129

Figure V

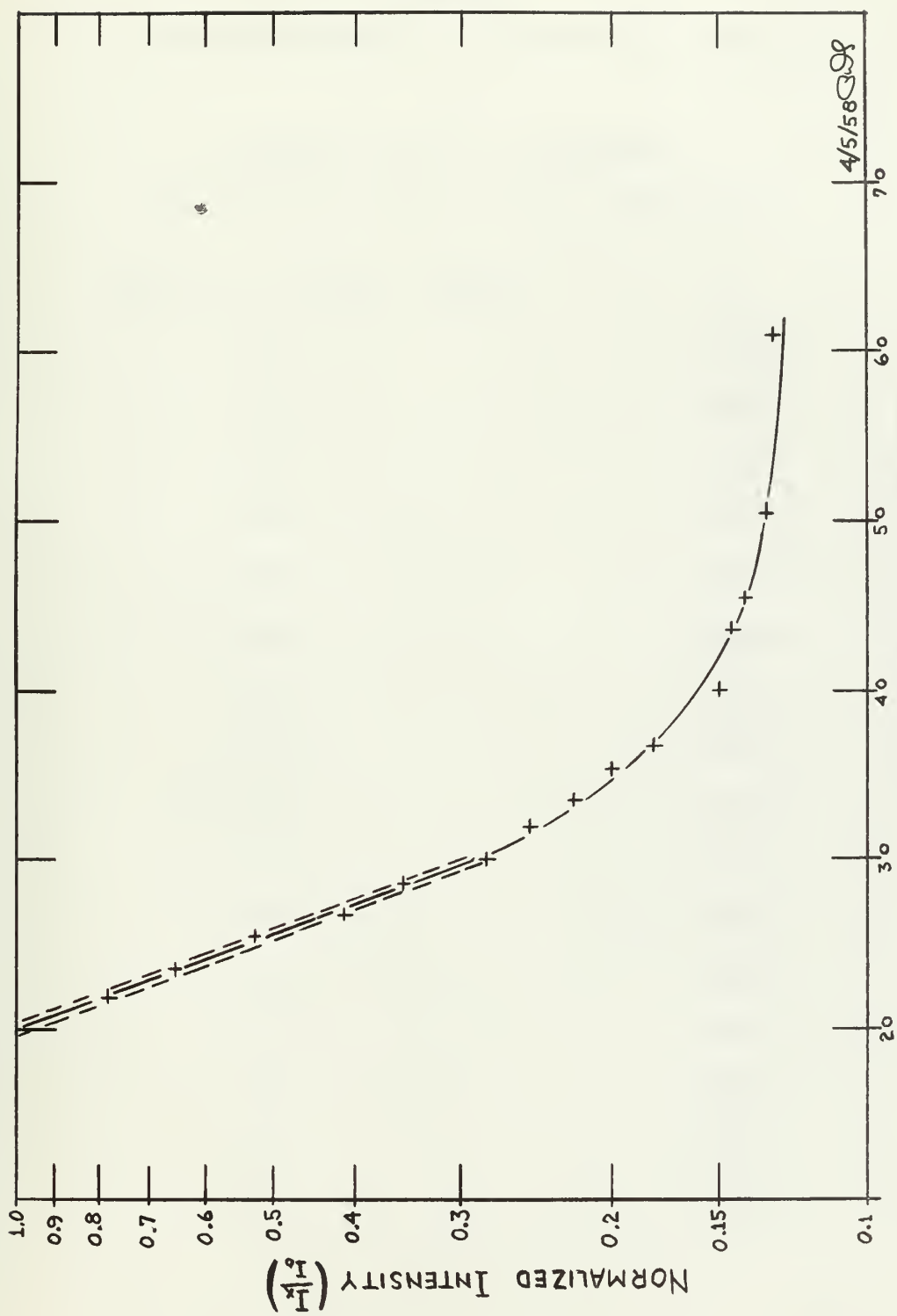

FIG V INTENSITY OF URANIUM L_{α_1} FLUORESCENT RADIATION VS CLADDING THICKNESS FOR ALUMINUM ON URANIUM - BACKGROUND INCLUDED

TABLE II

NORMALIZED URANIUM L FLUORESCENT INTENSITY

Vs.

ALUMINUM CLADDING THICKNESS

Background and Scattering Subtracted

Cladding Thickness (mils)	I
20.0	1.000
21.8	0.758
23.6	0.604
25.4	0.461
26.7	0.331
28.5	0.262
30.0	0.182
31.8	0.146
33.5	0.113
33.6	0.113
35.4	0.088
36.7	0.062
40.0	0.030
43.6	0.023
45.4	0.016
50.4	0.006

Figure VI

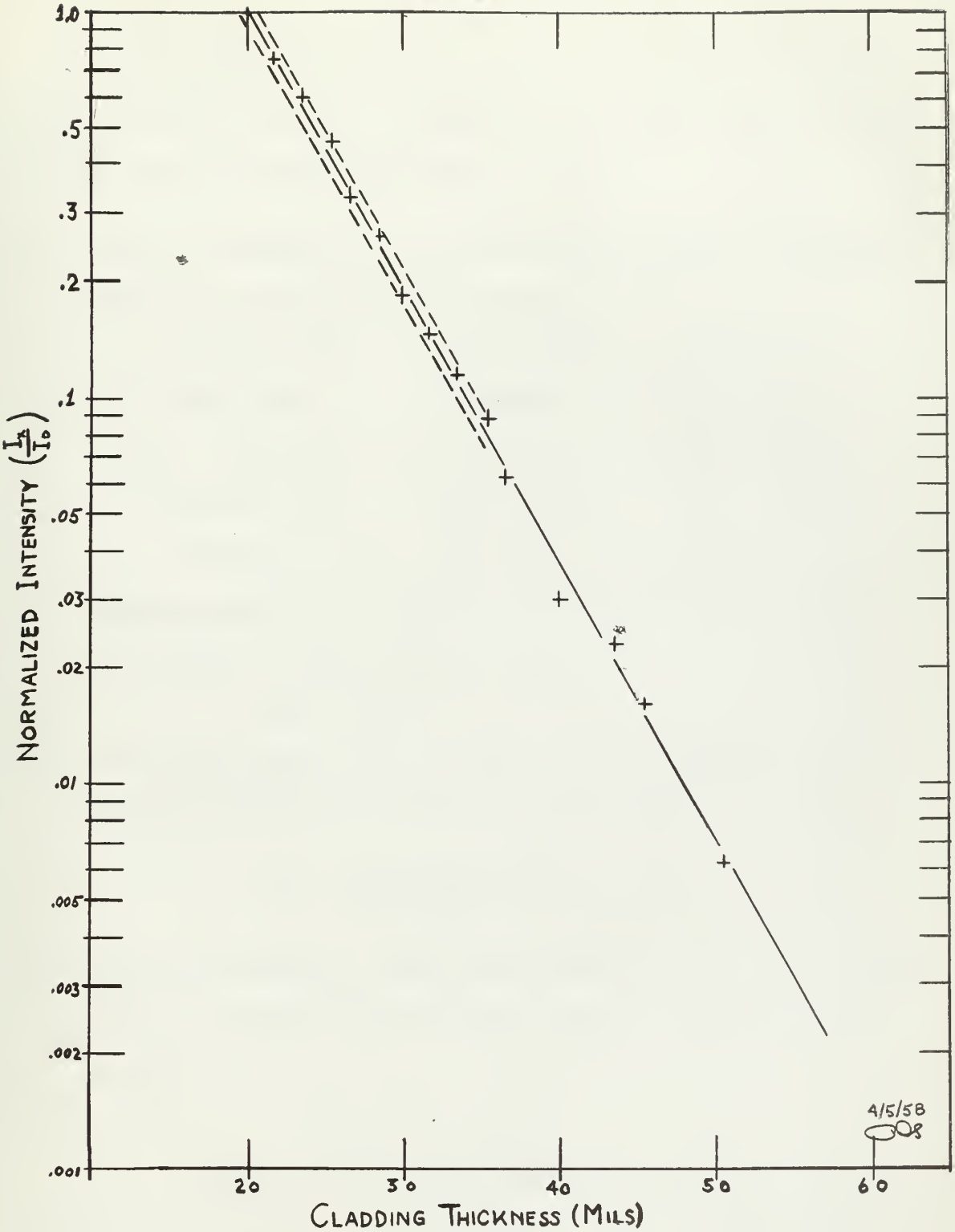

FIG VI INTENSITY OF URANIUM L_{α_1} FLUORESCENT RADIATION VS. CLADDING THICKNESS FOR ALUMINUM ON URANIUM - BACKGROUND SUBTRACTED

In order to check the reproducibility of the results recorded for aluminum cladding an "unknown" was measured using the following procedure:

1. The L_{α_1} intensity was recorded for a known reference specimen of 20.4 mils thickness.

elapsed time	total count	CPS
89.4 sec	102,400	1145.4

2. The L_{α_1} intensity was recorded for the "unknown".

elapsed time	total count	CPS
170.35 sec.	102,400	601.1

3. Entering Fig. V the normalized counting rate for 20.4 mils is read from the chart.

$$N_{NOR} = 0.96$$

4. The normalized counting rate for the "unknown" is determined from the reference specimen.

$$N_{NOR} = \frac{601.1\ (0.96)}{1145.4} = 0.504$$

5. Re-entering Fig. V the cladding thickness corresponding to a normalized counting rate of 0.504 is found to be:

$$t_{UNKNOWN} = 25.4 \text{ mils}$$

The "unknown" specimen was composed of four foils adding up to a total of 25.3 mils. The resulting error in this case was +0.1 mil, or 0.4%.

TABLE III

NORMALIZED URANIUM L FLUORESCENT INTENSITY

Vs.

ZIRCONIUM CLADDING THICKNESS

Cladding Thickness (mils)	I
0.0	1.000
2.0	0.017
4.0	0.000

TABLE IV

NORMALIZED URANIUM L FLUORESCENT INTENSITY

Vs.

STAINLESS STEEL CLADDING THICKNESS

Cladding Thickness (mils)	I
0.0	1.000
5.0	0.000

RESULTS

K FLUORESCENCE INVESTIGATION

TABLE V

NORMALIZED URANIUM K FLUORESCENT INTENSITY

Vs.

ZIRCONIUM CLADDING THICKNESS

Cladding Thickness (mils)	I				
	Run 1	Run 2	Run 3	Run 4	Run 5
5.0	0.882	0.914	0.907	0.902	0.882
10.0	0.766	0.799	0.810	0.825	0.794
15.0	0.739	0.726	0.746	0.772	0.752
20.0	0.698	0.629	0.682	0.652	0.695
25.0	0.588	0.593	0.603	0.611	0.591
30.0	0.502	0.516	0.539	0.520	0.506
35.0	0.461	0.495	0.466	0.479	0.495
40.0	0.457	0.455	0.424	0.434	0.455
50.0	0.393	0.395	0.412	0.402	0.408
59.0	0.343	0.368	0.352	0.352	0.353

Figure VII

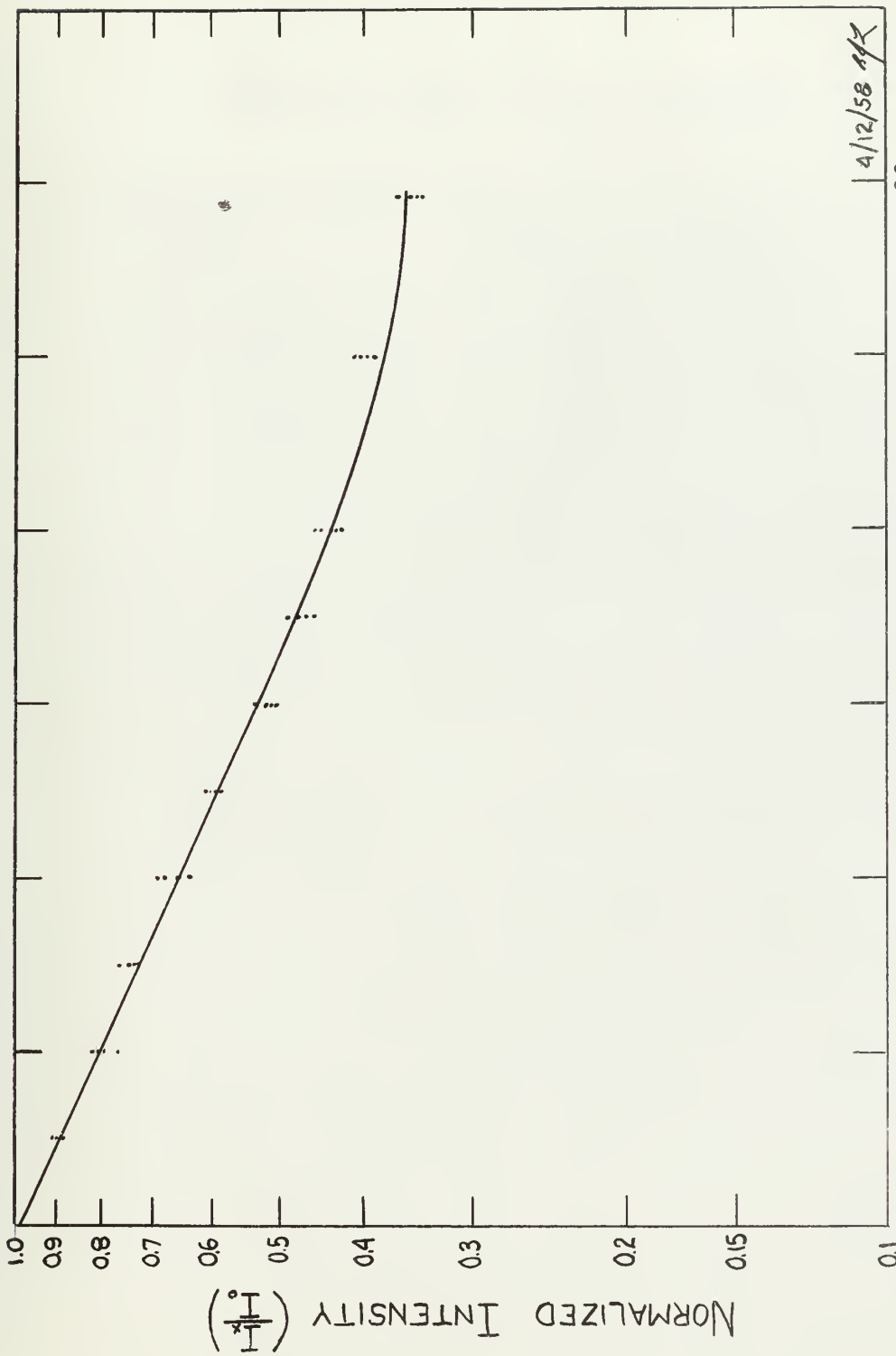

Fig VII Intensity of Uranium K Series Fluorescent Radiation vs Cladding Thickness – Zirconium on Uranium

TABLE VI

NORMALIZED URANIUM K FLUORESCENT INTENSITY

Vs.

STAINLESS STEEL CLADDING THICKNESS

Cladding Thickness (mils)	I		
	Run 1	Run 2	Run 3
5.0	1.023	1.062	1.062
10.0	1.000	0.984	1.016
20.0	1.016	1.054	1.039
30.0	0.976	0.976	0.967
40.0	0.984	0.951	1.000
50.0	0.985	0.976	1.023
60.0	0.951	0.985	0.976

Figure VIII

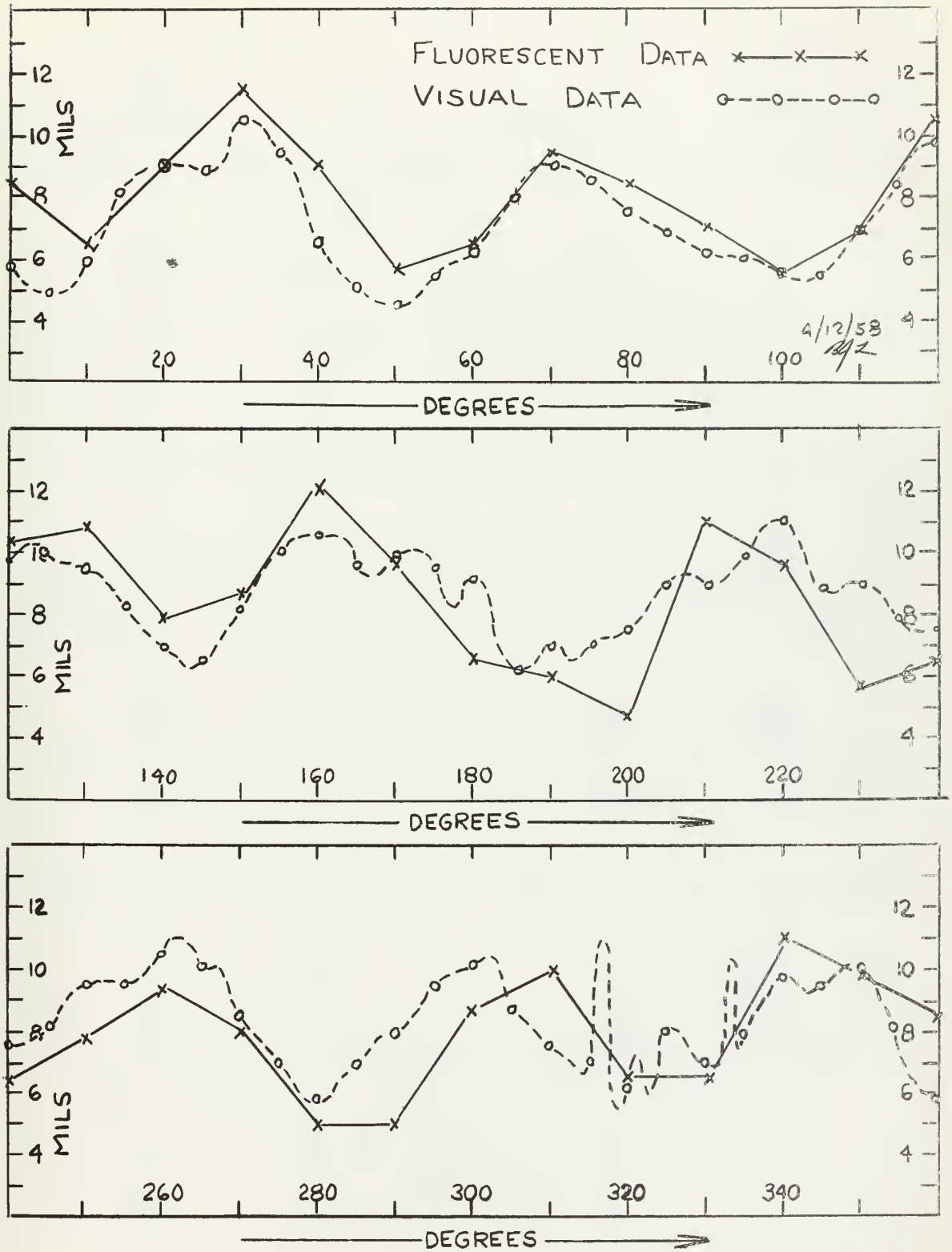

Fig. VIII Static Scan of Tubular Fuel Element and Visual Data of Nuclear Metals, Inc. for Tubular Specimen

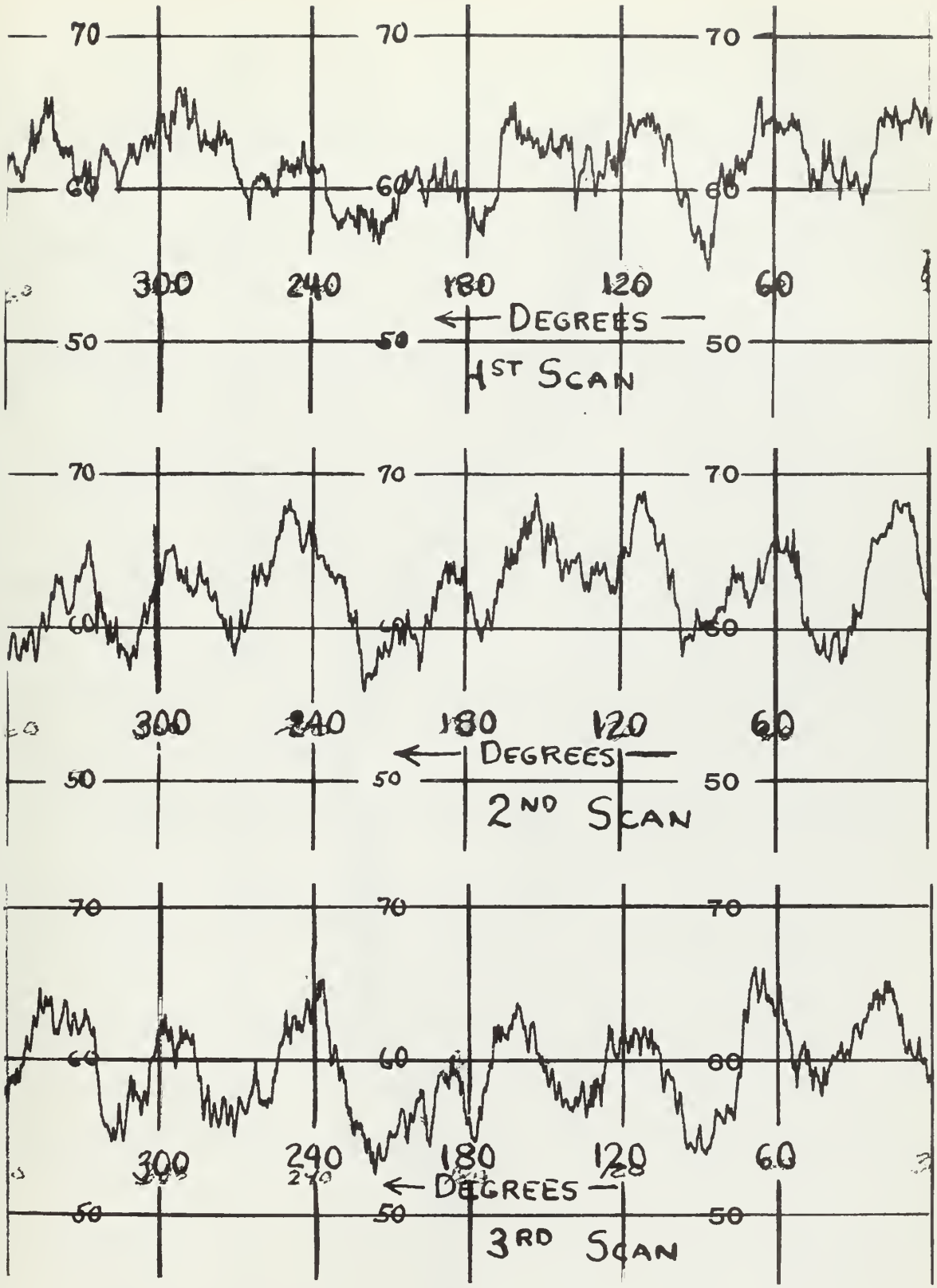

Fig. IX Rotational Scan of Tubular Fuel Element

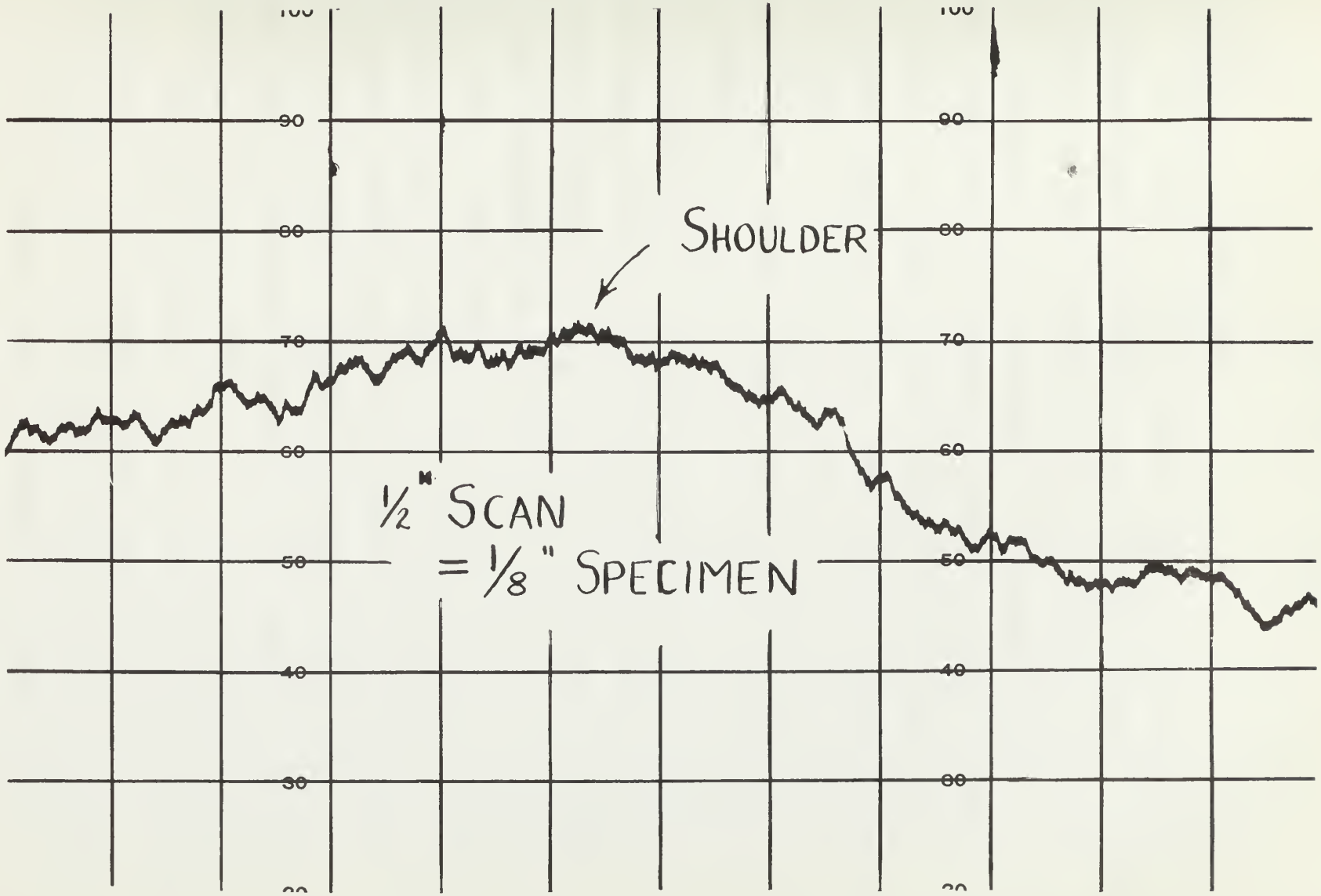

Fig. X Longitudinal Scan of Sectioned Cylindrical Fuel Element

DISCUSSION OF RESULTS

Uranium L Fluorescence:

The results clearly indicate that of the three cladding materials investigated only aluminum cladding, in the range of thickness desired, may be successfully measured by attenuation of the uranium L fluorescent series. The attenuation coefficients of stainless steel and zirconium are so high for this range of photon energy that they are essentially opaque, and, for the geometry in use, can only be measured to the order of one or two mils of cladding thickness. Optimizing the geometry so as to present the minimum cladding thickness to the incident and fluorescent X-ray beams would approximately double the range of cladding thickness that could be measured, while increasing the intensity and energy of the incident beam would permit measurements of stainless steel and zirconium of the order of six mils in thickness. By the same procedure the effective range of measurement of aluminum cladding could be increased to approximately a thirty mil range of cladding thickness, however, the accuracy of measurement would also be reduced due to the decrease in the effective linear attenuation coefficient.

From the analysis of the results of the investigation carried out for aluminum cladding with the uranium L fluorescent series the probable error of any one measurement in the cladding range of twenty to thirty mils is

$\pm$ 4.5% or approximately $\pm$ 1 mil. Since the statistical error was held to $\pm$ 0.31% by controlling the number of counts and the equipment operating point was stabilized to $\pm$ 0.1% by the voltage and current stabilizers the predominant error of approximately $\pm$ 4.5% can be assigned to the value for foil thickness. This assignment of an error of $\pm$ 1 mil to the effective thickness of cladding is reasonable when the method of assembly of a specimen is considered. Each specimen was assembled from several layers of foil, each foil measured by micrometer to within approximately $\pm$ 0.2 mil. A further error was introduced into the effective combined thickness of the specimen by a slight bowing of the foils in the specimen holder, and wrinkling of the thinner foils. The total cumulative error in effective foil thickness is unknown, but can be justifiably assumed to be $\pm$ 1 mil. With a carefully machined series of calibration specimens accuracies of better than $\pm$ 1% in the measurement of aluminum cladding could be expected, utilizing the uranium L_{α_1} spectral line and presently available equipment.

The probable error predicted by statistical analysis of the data appears to be rather large when compared with the error obtained in checking the cladding thickness of an "unknown" specimen. This apparent discrepancy can be reconciled if it is remembered that essentially all error was contained in the combined foil thickness of the specimen.

The "unknown" specimen, which was constructed in an identical manner to the specimens used to determine the calibration curve, had the same relative error as the reference specimens. This check serves to illustrate the reproducibility of the results, and the high order of accuracy which would be obtainable with an accurate series of calibration specimens.

Uranium K Fluorescence:

The results of the K series fluorescence investigation indicate that only zirconium may successfully be measured by attenuation of the uranium K series. The reasons that this technique could not be extended to stainless steel can be generally attributed to the fact that with reduced atomic number the scattering coefficient of the material increases in importance relative to the total attenuation coefficient. This increased scattering was sufficient to offset any decrease in the intensity of radiation due to attenuation of the uranium K series fluorescence.

For zirconium, the results of this investigation indicated that the range of cladding thicknesses that could be measured was of the order of zero to thirty mils of thickness. By an optimization of the geometry this range could be extended to approximately forty-two mils, however, the accuracy of measurement would be reduced due to a decrease in the effective linear attenuation coefficient.

From an analysis of the results of the investigation for zirconium, the probable error of any one measurement in the range of zero to thirty mils is $\pm$ 7.4 percent, or $\pm$2 mils in the upper limits of the zero to thirty mil range. The statistical error was held to $\pm$ 0.62 percent by controlling the number of counts. The predominant error of approximately 7.0 percent can be assigned to: 1) fluctuations due to instabilities in the operating equipment (See detailed procedure, K fluorescence), and 2) the method of assembling the test specimens. (See discussion of results, L fluorescence) As in the case of L fluorescence, accuracies of better than $\pm$3 percent could be realized with improved equipment. This would require adequately stabilized equipment and an accurately machined series of specimens.

A static scan of the tubular specimen (Fig. III) at intervals of ten degrees indicated an excellent correlation with the data furnished by Nuclear Metals, Inc. The results (Fig. VIII) not only clearly showed the eight fold symmetry of the extruded specimen, but also correlated within two mils of the visually observed thickness. The collimated beam used in the investigations (3/16") was of such area that any data obtained was necessarily representative of an average cladding condition of the area covered by the incident beam. With a more intense, more highly

focused X-ray beam it is believed that even closer correlation could be obtained.

Analysis of the rotating scan (Fig. IX) shows that the cladding material thickness ranges from five to thirteen mils, if we assume that the maximum intensity is given by the point of thinnest cladding. (See analysis of data) It is important to note that this correlation was obtained even at the relatively high rotational speed of one revolution per minute, and with the high instabilities encountered in the equipment. Of particular interest in the scan, is the sharp indication of changes in the cladding thickness and the clear indication of the eight fold symmetry of the tubular element.

A longitudinal scan (Fig. X) of the sectioned fuel element (Fig. IV) shows clearly the shoulder and the sharp increase in cladding thickness. No effort was made to correlate the scan with actual cladding thickness, however, this scan indicates that changes in cladding thickness can be detected even in the range of thirty to forty mils of cladding in a scanning operation.

It is believed that with construction of more adequately stabilized equipment, and the development of a more intense and highly focused incident X-ray beam, that considerably

more rapid and accurate scanning runs could be conducted. The above scanning runs serve to illustrate the feasibility of such a proposal.

SECTION B

COMPTON SCATTERING THEORY

The phenomenon of Compton scattering occurs whenever an incident photon is elastically scattered by an atomic or free electron. The general procedure employed in this section of the thesis was to direct a collimated beam of photons upon a target specimen and to measure the cladding thickness by correlation with the intensity of the scattered radiation. Other interactions which might occur due to the incidence of photons upon matter have been previously described in the Introduction and in Section A. Although these phenomena are taking place concurrently with the Compton scattering of photons, the method to be proposed confines itself to measurement of the scattered radiation alone. For this reason, the theoretical discussion is confined to that of Compton scattering and subsequent contributions to photon scattering theory.

The scattering of very-low energy photons was adequately described by the classical theory of J. J. Thomson [10]. However, as the energy of the incident photons approached $m_o c^2$, the rest mass of the electron, no correlation was obtained between scattered energy and the theoretically predicted scattering energy.

It remained for A. H. Compton [2] to demonstrate the relativistic nature of high energy photons. In order to explain the apparent discrepancies between theory and experiment, Compton assumed that the incident electromagnetic radiation could be considered as a quantum unit, and that the scattering process could be viewed as an elastic collision between the incident photon (the quantum unit of light) and a free electron. This collision was to be governed by the two basic laws of mechanics: 1- the conservation of energy, and 2-the conservation of momentum. Changes in the energy and momentum of the electron were to be considered relativistically. Assertion of these principles leads to the equation:

$$\frac{1}{h\nu} - \frac{1}{h\nu_o} = \frac{1}{m_o c^2} (1 - \cos \theta) \qquad (7)$$

where:

θ = angle of the scattered photon

$h\nu_o$ = energy of the incident photon

$h\nu$ = energy of the scattered photon

h = Planck's constant

ν = frequency of the photon (ν equals $\frac{\lambda}{c}$)

This expression may be written in the more conventional form:

$$\lambda - \lambda_o = \frac{h}{m_o c} (1 - \cos \theta) \qquad (8)$$

Equation (8) is the well known expression for the Compton shift. Careful experimentation by numerous acientists has proven the validity of the Compton theory.

The intensity of the scattered radiation for low energy photons ($h\nu \ll m_o c^2$) had been accurately described by the simple classical theory of J. J. Thomson [10] , however the intensity of scattered radiation proved to be much less than that predicted for the case of high energy photons. These discrepancies were resolved when Klein and Neshina [6] successfully applied Dirac's relativistic theory of the electron to the scattering problem and developed a wave-mechanical model which has shown substantial correlation with subsequent experiments. Following the development of the Klein-Neshina equations as shown by R.D. Evans [5] , it is shown that the differential collision cross section for incident unpolarized electromagnetic radiation is:

$$d({}_e\sigma) = \frac{r_o^2}{2} d\Omega \left(\frac{\nu'}{\nu_o}\right)^2 \left(\frac{\nu_o}{\nu'} + \frac{\nu'}{\nu_o} - \sin^2\theta\right) \quad (9)$$

where

$d\Omega = 2\pi \sin\theta \, d\theta$

$r_o^2 = e^2/m_o c^2$, the classical electron radius

ν' = frequency of scattered radiation

ν_o = frequency of incident radiation

The differential collision cross section $d({}_e\sigma)$ can be physically described as being the probability that an incident photon with energy $h\nu_o$, while passing through an absorber of such thickness that it contains one electron per square centimeter, will suffer a particular collision from which it will emerge with energy $h\nu'$, within a solid angle $d\Omega$ and at some angle θ from the direction of the incident photon.

If one considers the amount of energy carried out by the scattered photon then it may be simply represented by

$$d({}_e\sigma_s) = \frac{\nu'}{\nu_o} d({}_e\sigma) \qquad (10)$$

since the differential collision cross section represents the probability of the removal of an incident photon, with energy $h\nu_o$, from the collimated beam. Only the fractional part of the energy $h\nu'/h\nu_o$ is scattered, therefore, the differential scattering cross section, which is proportional to the energy scattered into the solid angle $d\Omega$ is simply ν'/ν_o multiplied by the differential collision cross section. In the case of incident unpolarized radiation this expression is:

$$d({}_e\sigma_s) = r_o^2 \, d\Omega \left(\frac{\nu'}{\nu_o}\right)^3 \left(\frac{\nu_o}{\nu'} + \frac{\nu'}{\nu_o} - \sin^2\theta\right) \qquad (11)$$

or allowing α to equal $h\nu_o/m_o c^2$ this may be rewritten:

$$d(\sigma_{es}) = r_o^2 \, d\Omega \left[\frac{1}{1 + (1 - \cos\theta)}\right]^3 \left(\frac{1 + \cos^2\theta}{2}\right) \left\{1 + \frac{\alpha^2(1 - \cos\theta)^2}{(1 + \cos^2\theta)[1 + \alpha(1 - \cos\theta]}\right\} \quad (12)$$

For low energy photons (i.e. - as α approaches the limiting value of zero) this expression reduces to the classical expression:

$$d(\sigma_{es}) = r_o^2 \, d\Omega \, \sin^2\theta \quad (13)$$

as proposed by J. J. Thomson [10].

The integrated probability, per electron, that a scattering event will occur is simply the integral of the differential collision cross section, equation (9), over all permissible values of θ. Performing the integration there is obtained:

$$\sigma_e = \int_0^\pi d(\sigma_e) = 2\pi r_o^2 \left\{\frac{1+\alpha}{\alpha^2}\left[\frac{2(1+\alpha)}{1+2\alpha} - \frac{1}{\alpha}\ln(1+2\alpha)\right] + \frac{1}{2\alpha}\ln(1+2\alpha) - \frac{1+3\alpha}{(1+2\alpha)^2}\right\} \quad (14)$$

This cross section, $_e\sigma$, represents the probability of a photon being removed from a collimated beam while passing through a material containing one electron per square centimeter. Tables and graphs of the differential and total cross sections, for Compton collisions have been given by Davisson and Evans [4] and Nelms [8].

It is interesting to note that in the previously presented expressions, the energy of the scattered photons is not a function of the scattering material, but only of the energy of the incident photon and the particular angle at which it is scattered.

In a thin foil of material with N atoms per cubic centimeter, and with each atom possessing Z electrons per atom, and of thickness dx , there will be NZ electrons/cm^3 and (NZ) dx electrons/cm^2 . In a collimated beam of intensity I , the change of intensity dI caused by the foil will be:

$$\frac{dI}{I} = (NZ)\, dx\, {}_e\sigma \qquad (15)$$

In calculating the attentuation of photons through any particular material it is convenient to use a Compton total linear attentuation coefficient σ which is defined as:

$$\sigma = (NZ)\, {}_e\sigma , \qquad (16)$$

Equation (15) may then be rewritten as:

$$\frac{dI}{I} = \sigma\!\!\!^{-}\, dx \qquad (17)$$

This expression is analogous to equation (1). The term μ in equation (1) refers to the total attentuation coefficient with respect to all type interactions of photons with matter, while the $\sigma\!\!\!^{-}$ in equation (17) refers to the attentuation caused by Compton scattering alone. $\sigma\!\!\!^{-}$ is, of course, part of the total linear attentuation coefficient μ .

Thus, it is seen that while the energy of the scattered photons is a function of the incident energy and the scattering angle, the intensity of the scattered radiation is a function of the intensity of the incident radiation, the density of the target material and the atomic number Z .

PROCEDURE

The general experimental procedure was to direct a collimated beam of photons upon the target specimen. Due to the large differences in atomic number and the densities of the base and the cladding material, it was proposed to evaluate the thickness of the cladding material by means of variations in the intensity of the scattered radiation. As is indicated by Figure I, in the energy regions under consideration the predominant mode of interaction of the incident photons with uranium will be that of a true absorption process, that is, that of X-ray fluorescence. In contrast, the principal mode of interaction in the cladding material will be that of Compton scattering. It is readily observable (see Figure I) that as the energy of the incident photons increases above approximately 1.0 Mev the principal mode of interaction for both the cladding and the uranium will be that of Compton scattering. It is to be expected, then, that for incident photons of the proper energy that there will be an increase of scattered radiation with an increase in cladding thickness.

In producing the scattered radiation of sufficient intensity and energy to be useful, various other phenomenon are also produced. These are respectively, the characteristic

series of the cladding element and its alloys and the characteristic series of the uranium. In order to correlate the thickness of the cladding material with the scattered radiation, it is necessary to resolve the scattered energy from the remainder of the polychromatic spectrum. In all phases of the photon scattering investigation a non-dispersive technique was utilized. As in the K fluorescence investigation a pulse height analyser was used for spectrum analysis. The remainder of the detection and analysis equipment is also identical with the equipment used in the K fluorescence investigations. (See Appendix A for details of the equipment.)

As in the case of the fluorescence investigations, the experiments conducted were purely a basic feasibility study and in all cases the equipment and the geometry utilized were not the most desirable in order to obtain optimum results.

The discussion of procedure for Compton scattering has been divided into two classifications: low and high energy photons. This division is actually synthetic in that the same theory is applicable in both energy regions, however, it facilitates discussion in that the source of the collimated beam and the geometry of the two experiments were different.

Low Energy Photon Scattering:

Equipment:

The equipment set-up for the low energy photon scattering investigation was identical with that used for K fluorescent "fixed count" tests. This resulted in a 90 degree scattering angle for the scattered photons. This angle was advantageous in that it removed the detector from the path of the incident X-ray beam, thus reducing background. Since at this photon energy scattering is becoming essentially anisotropic, the scattering angle is not critical with respect to scattered intensity.

Procedure:

The scattering portion of the spectrum reaching the detector from the target was separated from the uranium fluorescent radiation by setting the base line of the pulse height analyzer at the peak of the scattered spectrum, and reducing the window width to remove the uranium fluorescent portion of the spectrum above the base line. The X-ray unit was operated at 150 Kev to obtain the maximum counting rate and reduce the statistical error.

The intensity of the scattered radiation was recorded for various thicknesses of cladding foil over the uranium specimen. A total of five counting runs was made at each cladding thickness in an attempt to average out the fluctuations caused by variations of line voltage. By using a

combination of foils of known thickness, in a manner similar to the procedure followed for the fluorescent investigations, a relationship between scattered intensity and cladding thickness was determined for the various materials.

From data recorded during the K fluorescent investigation, it was seen that the variations of scattered intensity with zirconium cladding thickness was negligible, and, therefore, only aluminum and stainless steel were investigated by the technique of low energy photon scattering. (See Figure XIX for the variation of scattered intensity with zirconium cladding thickness.)

High Energy Photon Scattering Technique

A ten milli-gram radium capsule was used as a radiation source for the feasibility investigation of cladding thickness measurement utilizing the Compton scattering phenomenon. A larger, more mono-energetic source such as Cobalt 60 would have been preferred, however, with the use of a non-dispersive technique the radium source was considered satisfactory for a feasibility study.

The detection, recording and analysis equipment used in conjunction with this phase of the thesis investigation was indentical to that used in the K series fluorescence and low energy scattering investigations. Collimation of the gamma rays was accomplished by means of lead collimating ports. Both source and detector were thoroughly shielded to reduce the background to a minimal value. Figure XI illustrates the geometrical arrangement of source, specimen and detector. (See Appendix A for details of equipment.)

The cladding materials chosen for investigation were aluminum, 304 stainless steel and zirconium. In each case, a flat slab approximation was used to simulate the fuel element.

The procedure followed in this technique was similar to that followed in the other non-dispersive procedures. A scan of the energy spectrum as a function of base line voltage of the pulse height analyser was first made. (As in previous procedures, the dynode voltage was maintained at 900 volts to acquire maximum resolution.) The results of this scan were

negative in that the spectrum was flat and that no scattering peak could be resolved as in the case of the low energy photons. It was then decided to maintain the base line voltage of the pulse height analyser above the known fluorescent peak of the uranium series. With the window opened to its maximum value, the counting rate would then be proportional to the total scattered radiation whose energies were in excess of the K series of uranium.

A series of "fixed count" measurements for various known thicknesses of the several cladding materials were then made. These measurements are recorded in **Table IX.**

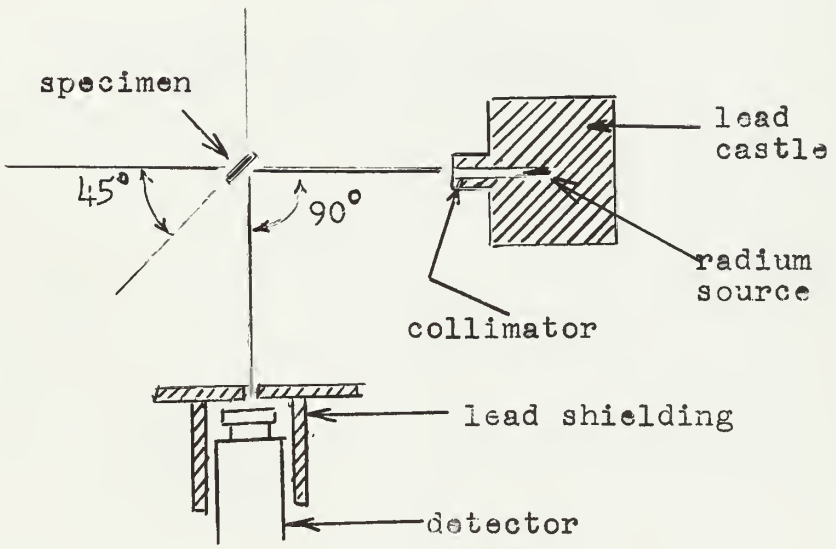

Figure XI Equipment Arrangement for High Energy Scattering Investigation

RESULTS

LOW ENERGY PHOTON SCATTERING

TABLE VII

NORMALIZED LOW ENERGY PHOTON SCATTERING INTENSITY

Vs.

ALUMINUM CLADDING THICKNESS

Cladding Thickness (mils)	Run 1	Run 2	Run 3	Run 4	Run 5
0.0	1.000	0.995	1.000	0.985	1.020
6.7	1.296	1.292	1.309	1.266	1.271
10.0	1.458	1.426	1.442	1.405	1.337
16.7	1.703	1.617	1.703	1.660	1.552
20.5	1.711	1.765	1.833	1.833	1.825
30.9	2.005	2.026	2.070	2.070	2.048
40.9	2.319	2.291	2.278	2.333	2.362
50.9	2.636.	2.619	2.533	2.619	2.637
60.9	2.984	2.939	3.031	2.939	3.055
69.3	3.319	3.080	2.810	3.031	2.984

Figure XII

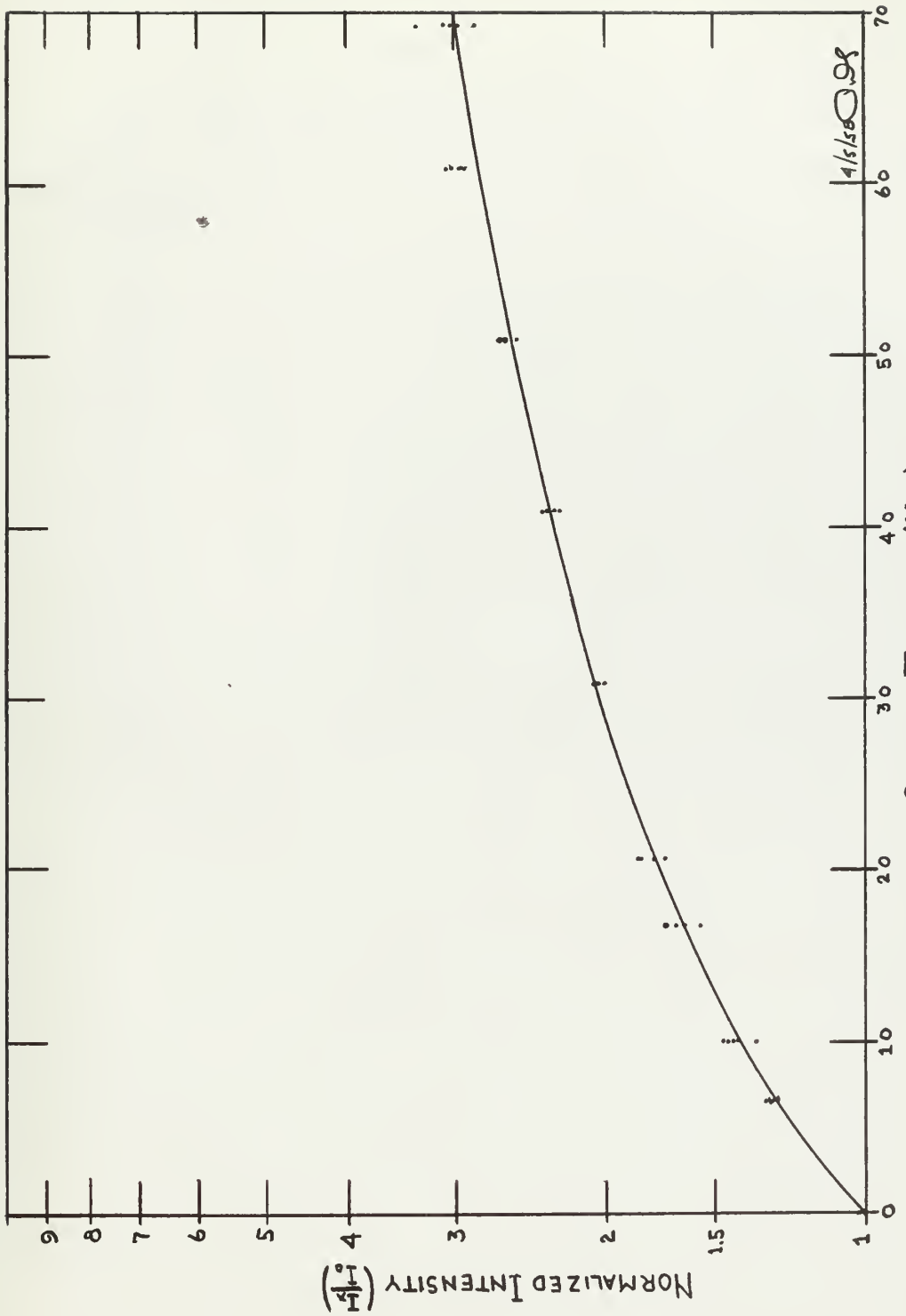

Fig XII Intensity of Scattered Radiation Vs. Cladding Thickness for Aluminum on Uranium - Low Energy Photons

TABLE VIII

NORMALIZED LOW ENERGY PHOTON SCATTERING INTENSITY

Vs.

304 STAINLESS STEEL CLADDING THICKNESS

Cladding Thickness (mils)	Run 1	Run 2	Run 3	Run 4	Run 5
0.0	1.040	1.003	1.009	1.033	1.000
5.0	1.379	1.390	1.379	1.407	1.407
10.0	1.848	1.772	1.727	1.828	1.772
15.0	2.085	2.178	2.164	2.178	2.072
20.0	2.358	2.460	2.408	2.391	2.342
30.0	2.693	2.693	2.803	2.827	2.693
40.0	3.026	3.053	2.948	2.974	2.923
60.0	3.257	3.196	3.226	3.353	3.257
70.0	3.454	3.386	3.320	3.353	3.353

Figure XIII

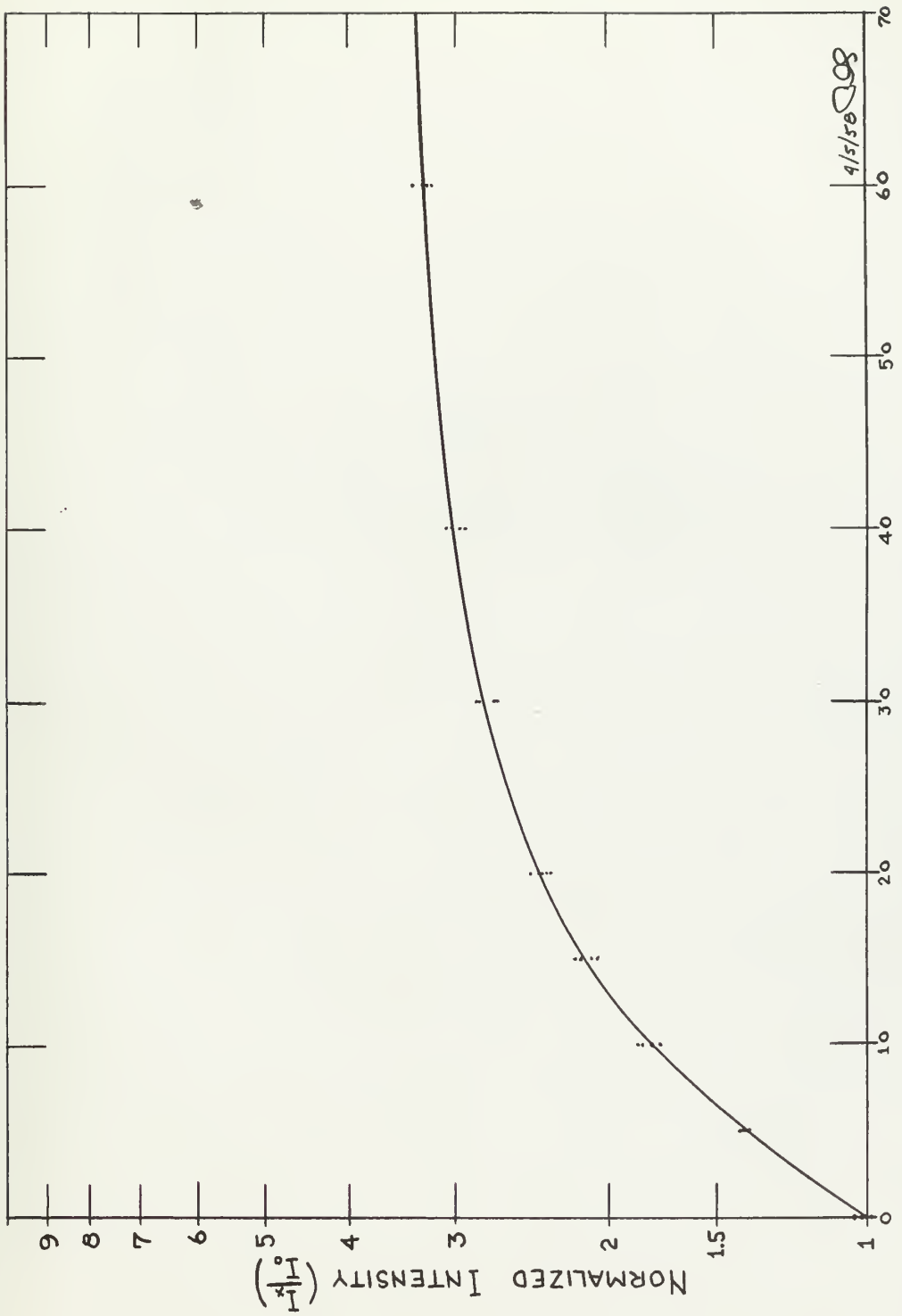

Fig XIII Intensity of Scattered Radiation Vs. Cladding Thickness for 304 Stainless Steel on Uranium - Low Energy Photons

RESULTS

HIGH ENERGY PHOTON SCATTERING

TABLE IX

NORMALIZED HIGH ENERGY PHOTON SCATTERING INTENSITY

Vs.

CLADDING THICKNESS OF ALUMINUM, STAINLESS

STEEL AND ZIRCONIUM

Cladding Thickness (mils)	I zirconium	I stainless
0.0	1.000	1.000
5.0	1.032	1.060
10.0	1.069	1.071
15.0	1.082	--
20.0	1.189	1.055
25.0	1.112	--
30.0	1.112	1.117
35.0	1.171	--
40.0	1.100	1.096
50.0	1.171	1.076
60.0	--	1.150
70.0	--	1.102

TABLE IX (cont.)

Cladding Thickness (mils)	I aluminum
0.0	1.000
7.0	1.018
10.0	1.053
20.0	1.045
30.0	1.091
40.0	1.192
50.4	1.130
60.9	1.216

DISCUSSION OF RESULTS

Low Energy Photon Scattering:

The normalized plots of scattering intensity vs cladding thickness for aluminum and stainless steel show considerable dispersion of the data. In some cases dispersion of the data was so great that no statistical difference could be found between readings differing by as much as 10 mils of cladding thickness. The average trend of the data, however, does show a definite and considerable change in scattering intensity with cladding thickness. The extreme variations in intensity for any one thickness of cladding can be mainly attributed to the X-ray source, since during the runs variations of as much as 16 percent in the X-ray tube input current were experienced.

The experimental plot of scattered intensity vs. cladding thickness is in good agreement with theoretical considerations (see Appendix C) and it is the conclusion of the authors that the curve passed through the data points represents the relationship that could be obtained with well stabilized equipment. The relationship between scattered intensity and cladding thickness is extremely dependent upon the energy of incident radiation and the geometry of the experiment, and the curves, therefore, are applicable only to the geometry used.

The accuracy that can be obtained by this technique is dependent upon the stability of the source and the scattering intensities obtainable. As indicated in Figures XII and XIII the accuracy decreases with increasing cladding thickness.

High Energy Photon Scattering:

Analysis of the data in the investigation for high energy photon scattering indicated no consistent statistical difference in intensity of the scattered radiation vs. variations in cladding thickness.

This fact can be explained in that for high energy photons the scattering mechanism is the predominant mechanism in both the cladding material and the uranium. (See Fig. I). For low cladding thicknesses the cladding material is essentially transparent to the incident high energy photons. The principal scattering takes place from the uranium. This softer, scattered radiation from the uranium now experiences relatively more attenuation by the cladding material due to the increase of the attenuation coefficient with decreasing photon energy. An increase in cladding thickness causes more appreciable attenuation and scattering in the incident beam and a relative loss of scattering from the uranium base. The overall effect for variations of cladding thickness is one of relatively little change.

The observed data correlates well with the results predicted by equation (18).

CONCLUSIONS

Based on the results of the various studies, the authors have reached the following conclusions:

1. The thickness of cladding on uranium fuel elements may be successfully measured by the application of the L fluorescent, K fluorescent or low energy Compton scattering technique, depending upon the atomic number and density of the cladding material.

2. To successfully measure cladding thickness by the above techniques the recording and analyzing equipment, and the exciting source should be stabilized to within one percent of the normal operating point of the equipment. The intensity of the exciting source should be as high as possible to reduce the statistical error.

3. Materials of low atomic number and density, such as aluminum, can be measured with accuracies of better than one percent at a cladding thickness of thirty mils, employing the uranium L fluorescent technique. Equipment of adequate stability to obtain this accuracy is now available.

4. Cladding materials of high atomic number and density, such as zirconium, can be successfully measured by the

application of the uranium K fluorescent technique. Presently available industrial X-ray equipment is not suitable for the determination of cladding thickness by uranium K fluorescence since it is not adequately stabilized. With adequately stabilized equipment an accuracy of measurement of three percent at thirty mils of zirconium cladding could be expected.

5. Cladding materials of moderately high atomic number, such as stainless steel, may be successfully measured by the uranium L fluorescent technique in the range of cladding thickness from zero to ten mils, depending upon the geometry employed. Within this range of cladding thickness accuracy of measurement of 1% could be obtained. For the measurement of cladding thickness greater than ten mils the technique of Compton scattering of incident photons of the order of 100 Kev may be applied, which will permit measurements with accuracies of approximately five percent at thirty mils of cladding thickness. Industrial X-ray equipment presently available is not suitable as the photon source, since the equipment is not adequately stabilized.

6. Cladding thickness determination by low energy photon scattering is not considered feasible for the cladding materials of low and high atomic number, since the application of the L or K fluorescent techniques will permit greater accuracy of measurement.

7. The scanning experiments conducted on the tubular fuel element indicate that the techniques of L and K fluorescence, and low energy photon scattering can be utilized in a continuous scanning process which would have industrial application as a quality control process.

RECOMMENDATIONS

Based on the results of the various investigations the authors make the following recommendations:

1. That studies be made to determine the extent to which presently available industrial X-ray units may be stabilized. Excitation equipment to be used for cladding thickness determination should be stabilized to within one percent.

2. That studies be made to determine methods of application of the techniques of X-ray fluorescence and low energy photon scattering to a continuous quality control process. One possibility would be a counting rate circuit used in conjunction with a gating circuit set for low and high tolerance levels.

APPENDIX A

DETAILED PROCEDURE

L Fluorescence Procedure:

Equipment:

The equipment used in the investigation of cladding thickness determination by excitation of L fluorescence of uranium is listed below. Figure XIV shows the details of the X-ray spectroscope used in the fluorescent analysis, while Figure XV shows the arrangement of the recording equipment in the Electronic Circuit Panel.

A. Analyzing Equipment

The analyzing equipment employed for the L fluorescent investigation was a lithium fluoride crystal spectrometer designed for fluorescent analysis. The exciting X-ray source (with a variable input from 0-50 Kev), specimen holder and crystal spectrometer is a combined table-top unit manufactured by North American Phillips Company, type 52157. The X-ray tube input is regulated by electronic voltage and current stabilizers maintaining tube input current to within $\pm$ 0.1% of the assigned value.

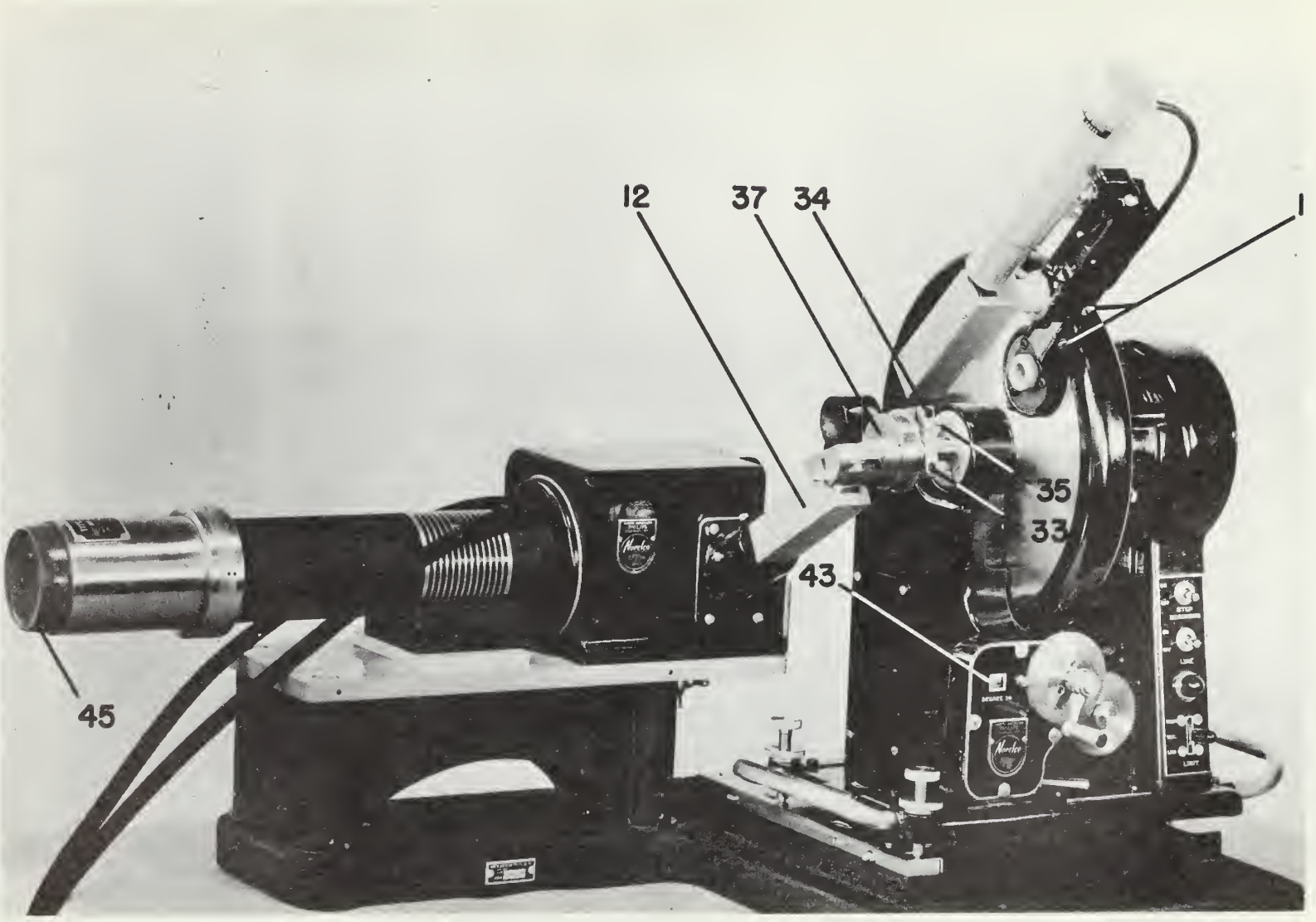

Fig. XIV X-ray Spectroscope

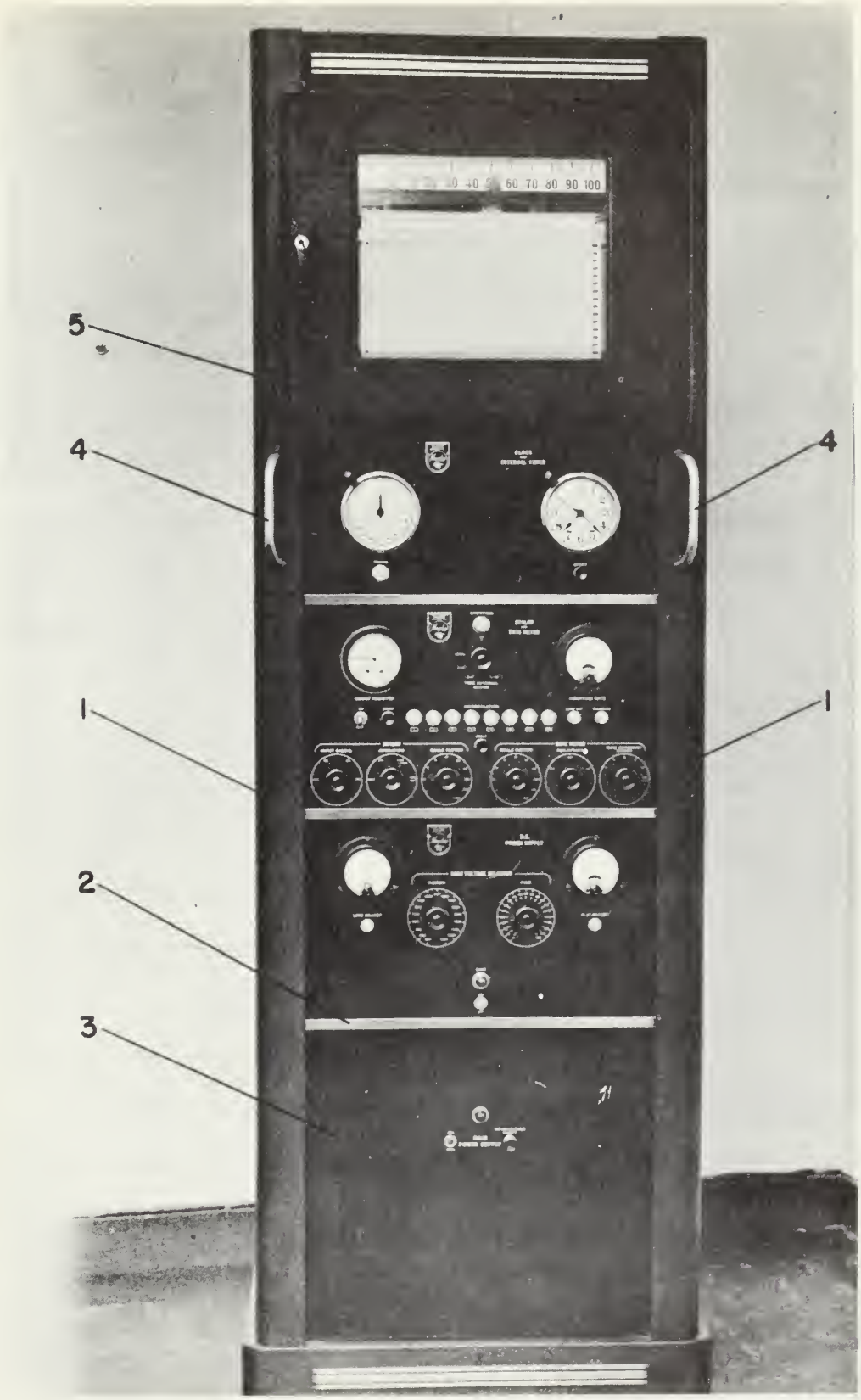

Fig. XV Electronic Circuit Panel

B. Detecting Device

The detecting device employed to count the fluorescent radiation was a thallium activated, sodium iodide scintillation counter. The quantum counting efficiency of the detector is approximately 99% for the L_{α_1} spectral line. The scintillation detector, photo-multiplier tube and preamplifier was a packaged unit manufactured by Norelco Manufacturing Company, type 52245, and was mounted directly on the goniometer arm of the crystal spectrometer. The fluorescent radiation from the specimen was collimated by a Soller Slit arrangement that was integral with the crystal spectrometer.

C. Recording Equipment

The following recording equipment was employed in analyzing the output of the scintillation head.

1. A Scintillation/Proportional Unit, Norelco type 42234, containing:
   a. a linear pulse amplifier
   b. amplitude discriminator
   c. high speed binary counting stages (not used due to malfunction)
2. Phillips Electronic Circuit Panel No. 12048, containing:
   a. Brown Recorder
   b. Clock and Interval Timer
   c. Scaler-Rate Meter
   d. D.C. Power Supply
   e. Electronic Stabilizer

Prior to the commencement of data runs a test was performed to check upon the randomicity of results. This check was made by performing a Chi-Squared test. Should the Chi-Squared test indicate non-randomicity of data the equipment would be checked for malfunction or spurious response. The test procedure followed is outlined by R.D. Evans.[5]

s fold scale = 6400 $\quad\quad$ $\bar{t}$ = mean counting time

t_i = time for 6400 counts (sec) $\quad\quad$ n = degrees of freedom

$P(\chi^2)$ Probability function

listed in Evans[5]

t_i	$\bar{t}/t_i$	$\bar{t}/t_i - 1$	$(\bar{t}/t_i - 1)^2 10^6$
12.75	0.986	0.014	196
12.59	0.999	0.001	1
12.83	0.979	0.021	442
12.60	0.997	0.003	9
12.50	1.005	0.005	25
12.48	1.006	0.006	36
12.63	0.995	0.005	25
12.37	1.018	0.018	324
12.48	1.006	0.006	36
12.49	1.006	0.006	36

$$\bar{t} = \frac{\sum t_i}{\sum 1} = 12.57 \qquad \sum (\bar{t}/t_i - 1)^2 = 1130 \times 10^{-6}$$

$$\chi^2 = s \sum (\bar{t}/t_i - 1)^2 = 7.24$$

$$F = n - 1 = 9$$

$$P(\chi^2) = 0.6$$

A $P(\chi^2)$ of 0.6 is indicative of good randomicity of data, indicating that the equipment is operating properly.

In order to find the optimum operating voltage for the photomultiplier tube a plot of counting rate vs. dynode voltage was determined for the L_{α_1} spectral line. The operating point chosen for future data runs was 885 volts, since at this point small fluctuations in dynode voltage have a minimum effect on counting rate.

K Fluorescence Procedure:

The equipment used in conjunction with the investigation of cladding thickness measurements by attenuation of uranium K series fluorescence is, with the exception of the analyzing device used, identical to the equipment used in the L fluorescence procedure.

The analyzing device employed in lieu of a crystal spectrometer was a pulse height analyzer. It is commercially available from the Atomic Instrument Company, model number 505. The base line had a range of from zero to 100

volts. The window width was variable from zero, to the condition in which it would accept all pulses with amplitude greater than the base line voltage. A block diagram of the circuitry employed is:

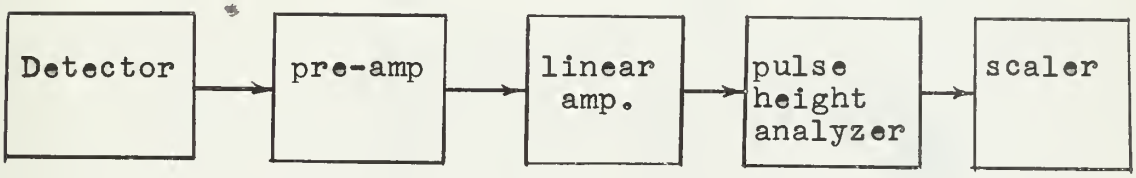

Figure XVI Block Diagram of Circuitry - K Fluorescent Investigation

Prior to commencing data runs it was necessary to optimize the equipment settings in order to realize the maximum resolution between the uranium K series fluorescent radiation and the general scattering from the uranium and the overlaying cladding material. This was accomplished by making scanning runs of the energy spectrum for both uranium and the cladding material. These scanning runs were superimposed and resolution of peaks was determined as a function of photomultiplier dynode voltage. A representative plot is shown in Figure XVII . It was determined that peak resolution increased with increasing dynode voltage. Based on the above procedure, the dynode voltage selected for future data runs was 900 volts.

It is interesting to note that the peak of the cladding

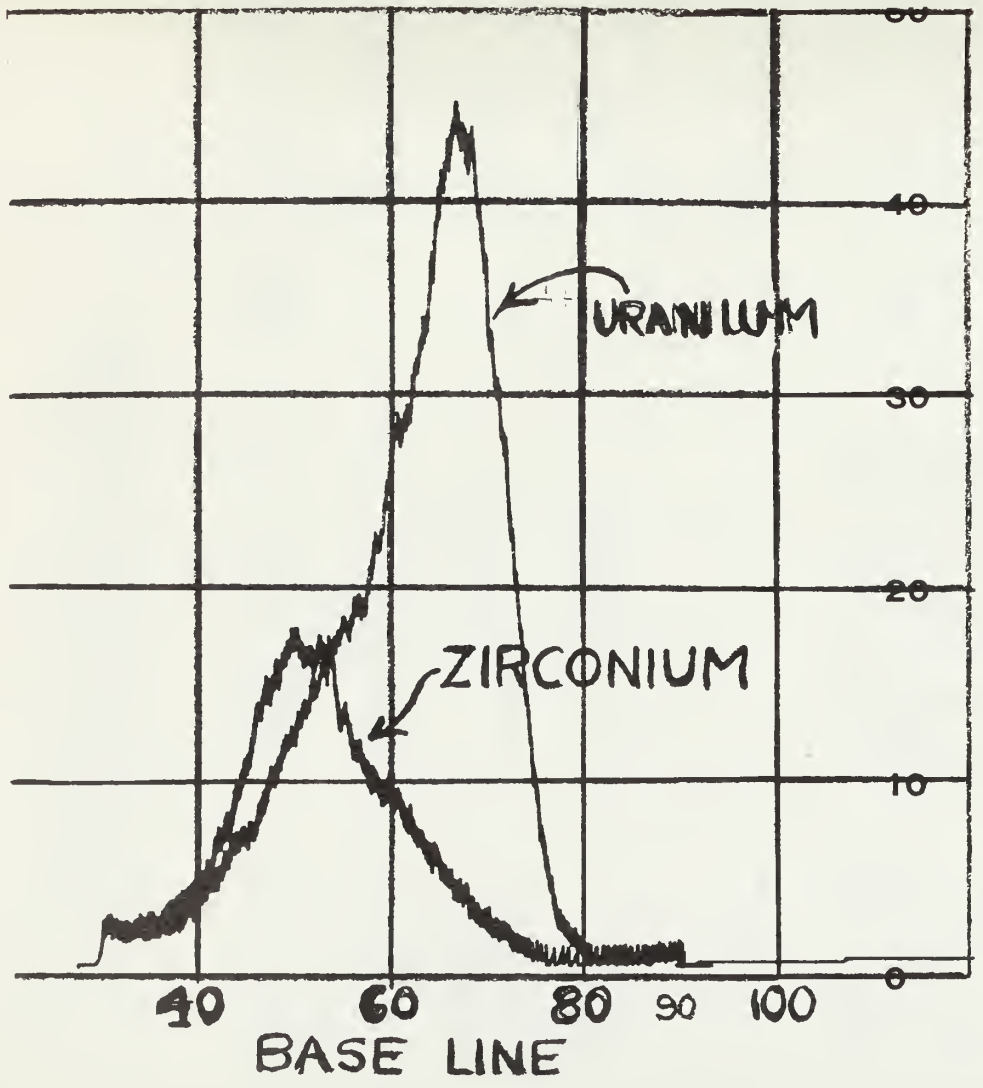

Fig. XVII Pulse Height Distribution of Energy Spectrum from Uranium and Zirconium

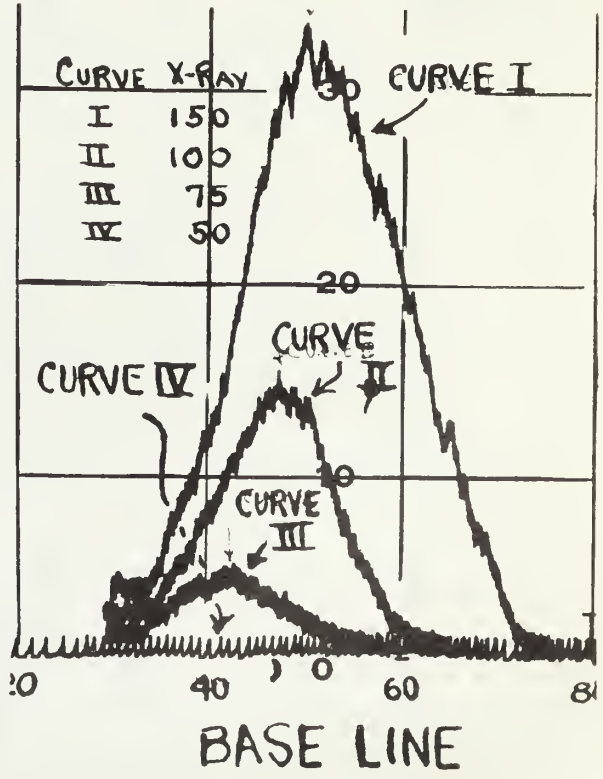

Fig. XVIII Pulse Height Distribution of Energy Spectrum from Zirconium - Varying X-ray Voltage

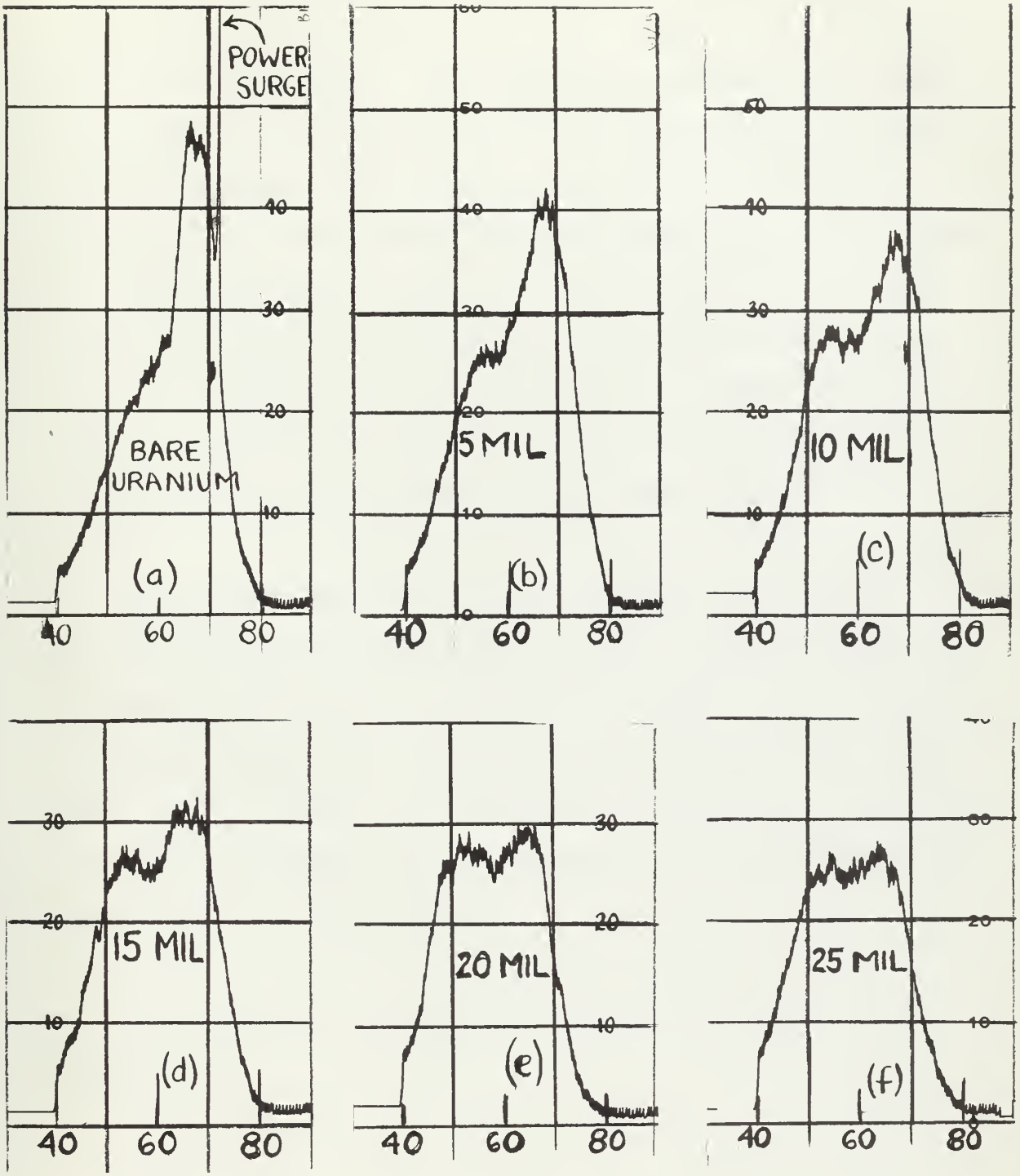

Fig. XIX Pulse Height Distribution of Energy Spectrum of Zirconium on Uranium - Varying Thickness of Zirconium

material is the result of scattered radiation rather than a fluorescent peak of the cladding material. This is indicated by Figure XVIII . The dynode voltage was held steady at 900 volts, and a series of scans of the zirconium were made at varying X-ray voltages. As the X-ray voltage decreased the peak shifted steadily down scale, and reduced in amplitude. This result is clearly indicative that the peak is the result of primary scattered radiation rather than a fluorescent peak of the material. While the scans shown are those for zirconium, corresponding traces, with identical peaks, were found for stainless steel.

Following completion of the determination of the optimum photomultiplier dynode voltage, scans were taken of the uranium with varying thicknesses of the cladding material overlaid. Figure XIX indicates a representative series of scans. It is clearly evident that for increasing thickness of zirconium increasing attenuation of the uranium K series fluorescence is taking place.

The geometrical arrangement of the equipment was as shown:

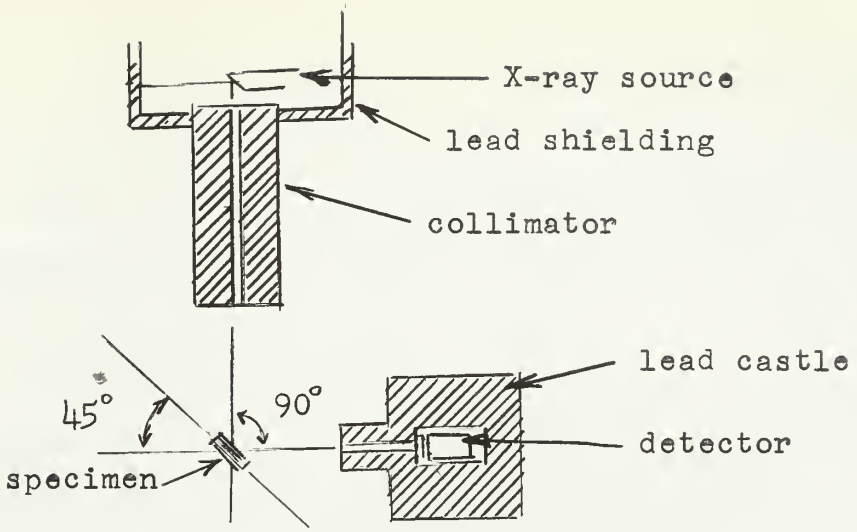

Figure XX Equipment Arrangement - K Fluorescent Investigation

In accord with the information gained from the preliminary scanning runs the base line voltage was set at an operating point of 67 volts and the window width at 3.0 volts. This setting essentially encompassed the fluorescent peak of the K series of uranium and blocked all scattered radiation.

Prior to the commencement of data runs a Chi-Squared test was made to check randomicity of results. (See L fluorescence procedure - Appendix A) Proper operation of the equipment was indicated. A series of 25,600 counts were recorded for varying thicknesses of the cladding materials. This data is presented in Tables XVII, XVIII and XIX.

Following completion of the static runs on the simulated flat plate specimen, a series of static runs were

made on a tubular fuel element (Fig. III) which was furnished by Nuclear Metals, Inc. The data obtained from these runs is presented in Table XX. The geometrical arrangement of the tubular fuel specimen is shown below:

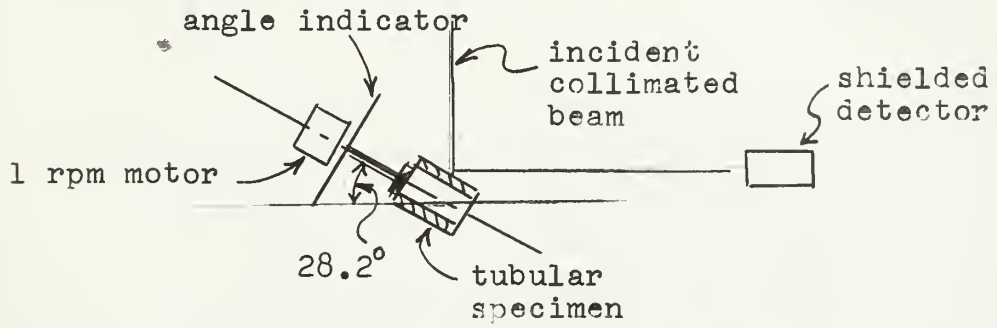

Figure XXI Specimen Arrangement - Rotational Scan

To determine the industrial feasibility of this process as a quality control measure the tubular specimen was scanned at a rotational speed of one revolution per minute. This data was continuously recorded on a Brown strip recorder. (Fig. IX)

A longitudinal scan of a sectioned cylindrical fuel element (Fig. X) was also made. The geometrical arrangement employed for the longitudinal scan was as shown below:

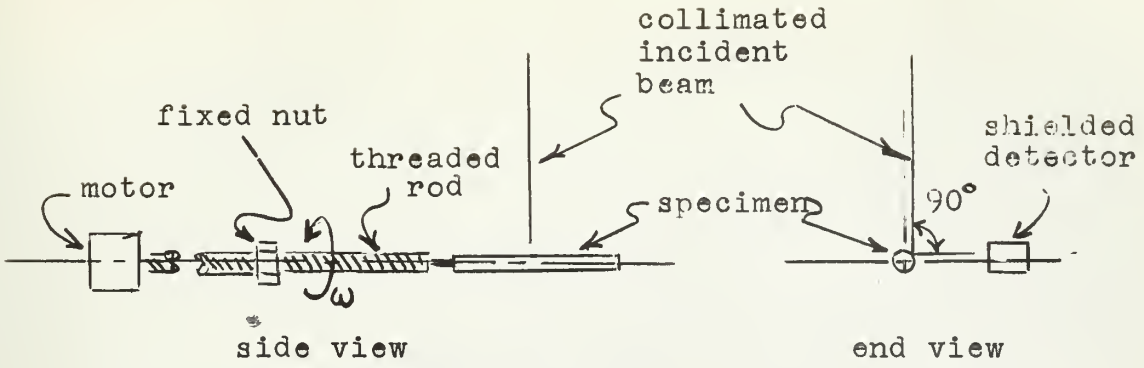

Figure XXII Specimen Arrangement - Longitudinal Scan

The results of this scan were continuously recorded on a Brown strip recorder. (Fig. X)

Some of the instabilities in the equipment are particularly well illustrated by Figure XIXa . Line surges and voltage instabilities consistently created great variations in the counting rate.

APPENDIX B

RECORDED DATA

TABLE X

Scattering Intensity from Aluminum with no Uranium Backing

L Fluorescent Investigation

X-ray Unit - 45 Kev, 30 ma. Total Count - 102,400

Cladding Thickness (mils)	Counting Time (sec)
20.0	855.8
30.0	796.6
40.0	769.6
50.4	754.5
60.9	740.2

TABLE XI

General Room Background

L Fluorescent Investigation

Total Count	Counting Time (sec)
10,000	1816.6

TABLE XII

L Intensity for Aluminum Cladding on Uranium Backing

L Fluorescent Investigation

X-ray Unit - 45 Kev, 30 ma. Total Count - 102,400

Cladding Thickness (mils)	Counting Time (sec)
20.0	95.1
21.8	120.9
23.6	146.0
25.4	180.7
26.7	231.0
28.5	270.6
30.0	338.8
31.8	380.3
33.5	429.9
33.6	429.0
35.4	474.9
36.7	535.8
40.0	633.8
43.6	656.1
45.4	684.4
50.4	722.7
60.9	737.2

TABLE XIII

Scattering Intensity from Zirconium with no Uranium Backing

L Fluorescent Investigation

X-ray Unit - 25 Kev, 12 ma. Total Count - 1600

Cladding Thickness (mils)	Counting Time (sec)
2.0	108.4
4.0	104.9
5.0	104.0

TABLE XIV

L Intensity for Zirconium Cladding on Uranium Backing

L Fluorescent Investigation

X-ray Unit - 25 Kev, 12 ma.

Cladding Thickness (mils)	Counting Time (sec)	Total Count
0.00	62.5	51,200
2.00	440.7	12,800
4.00	99.5	1,600
5.00	97.3	1,600

TABLE XV

Scattering Intensity from Stainless Steel with no Uranium Backing - L Fluorescent Investigation

X-ray Unit - 25 Kev, 12 ma. Total Count - 1,600

Cladding Thickness (mils)	Counting Time (sec)
5.0	191.6
10.0	193.4

TABLE XVI

L Intensity for Stainless Steel Cladding with Uranium Backing - L Fluorescent Investigation

X-ray Unit - 25 Kev, 12 ma.

Cladding Thickness (mils)	Counting Time (sec)	Total Count
0.00	63.4	51,200
5.0	188.2	1,600
10.0	196.2	1,600

TABLE XVII

K Fluorescent Intensity for Stainless Steel Cladding with Uranium Backing - K Fluorescent Investigation

Pulse Height Analyzer - Base Line = 67 volts

Window Width - 3.0 volts

X-ray Unit - 150 Kev, 5 ma. Dynode Voltage - 900 volts

Total Count - 25,600

Cladding Thickness (mils)	Counting Time (sec)		
	Run 1	Run 2	Run 3
0.0	12.6	12.6	12.5
5.0	12.9	13.4	13.4
10.0	12.6	12.4	12.8
20.0	12.8	13.3	13.1
30.0	12.3	12.3	12.2
40.0	12.4	12.0	12.6
50.0	12.5	12.3	12.9
60.0	12.0	12.5	12.3

TABLE XVIII

K Fluorescent Intensity for Zirconium Cladding with Uranium Backing - K Fluorescent Investigation

Pulse Height Analyzer - Base Line - 67 volts

Window Width - 3.0 volts

X-ray Unit - 150 Kev, 5 ma. Dynode Voltage - 900 volts

Total Count - 25,600

Cladding Thickness (mils)	Counting Time (sec)				
	Run 1	Run 2	Run 3	Run 4	Run 5
5.0	14.4	13.9	14.0	14.1	14.4
10.0	16.6	15.9	15.7	15.4	16.0
15.0	17.2	17.5	17.0	16.5	16.9
20.0	18.2	20.2	18.6	19.5	18.3
25.0	21.6	21.4	21.0	20.8	21.5
30.0	25.3	24.6	23.5	24.5	25.1
35.0	27.5	25.6	27.2	26.4	25.6
40.0	27.8	27.9	30.0	29.3	27.9
50.0	32.3	32.1	30.9	31.6	31.1
59.0	37.0	34.5	36.1	36.1	35.9

TABLE XIX

K Fluorescent Intensity for Bare Uranium Specimen

K Fluorescent Investigation

Pulse Height Analyzer - Base Line - 67 volts

Window Width - 3.0 volts

X-ray Unit - 150 Kev, 5 ma. Dynode Voltage - 900 volts

Total Count - 25,600

Run Number	Counting Time (sec)
1	12.8
2	12.2
3	12.7
4	12.7
5	13.0
6	12.6
7	12.4
8	13.1

TABLE XX

Fluorescent radiation from tubular element. Total counts per run- 25,600.

Angular Orientation (Degrees)	elapsed time (sec)						
	Run 1	Run 2	Run 3	Run 4	Run 5	Run 6	Run 7
0	41.18	40.88	40.96	41.15	41.23	41.58	41.60
10	39.66	39.76	39.88	39.41	39.34	39.32	39.33
20	40.81	41.78	42.40	42.39	42.79	41.33	41.82
30	44.88	44.40	44.20	44.90	44.42	44.00	44.56
40	41.17	41.91	41.50	42.07	41.65	41.62	42.28
50	38.60	38.54	38.51	38.44	38.53	38.86	38.70
60	40.19	39.20	39.53	39.79	39.34	39.48	39.22
70	43.24	42.89	42.47	42.19	40.98	41.49	42.38
80	41.30	40.80	40.92	41.37	41.40	41.43	41.17
90	39.17	39.37	38.78	39.14	39.70	40.54	40.63
100	38.42	37.95	38.67	38.38	38.50	38.28	38.42
110	39.96	40.32	40.67	39.52	40.63	39.54	39.49
120	43.59	42.95	43.00	44.25	43.30	43.02	42.87
130	43.02	43.58	43.37	43.45	44.60	44.60	44.06
140	41.55	40.02	39.84	41.60	41.07	40.78	40.60
150	42.68	42.62	42.10	41.05	41.11	40.68	40.80
160	44.70	45.10	45.84	45.62	45.30	44.70	45.49
170	42.87	42.52	42.78	42.51	42.86	42.31	42.61
180	40.07	39.95	39.68	39.48	39.90	39.57	39.01

Angular Orientation (Degrees)	elapsed time (sec)						
	Run 1	Run 2	Run 3	Run 4	Run 5	Run 6	Run 7
190	38.21	39.30	38.89	38.54	38.40	38.98	39.30
200	40.40	40.58	39.68	40.32	40.42	40.35	40.93
210	43.37	43.81	43.82	44.08	44.28	44.58	44.11
220	42.30	42.51	43.20	41.70	43.50	42.60	42.56
230	38.40	39.02	38.88	38.78	38.42	38.36	38.57
240	38.38	39.60	39.61	39.28	39.23	39.48	39.00
250	40.20	40.88	40.46	40.90	40.70	41.15	40.93
260	42.65	42.19	41.90	42.07	41.64	42.23	42.18
270	41.12	41.28	41.41	40.90	40.42	40.38	40.36
280	38.30	37.95	38.58	37.98	37.30	38.22	37.95
290	39.90	39.66	40.05	40.04	39.50	40.19	39.78
300	41.51	41.25	41.51	42.12	41.57	41.60	41.68
310	42.76	42.87	43.40	42.34	43.10	43.54	43.39
320	39.58	39.99	39.50	39.71	39.84	39.25	39.50
330	39.48	39.81	39.58	39.60	39.38	39.82	39.68
340	43.46	43.69	44.32	43.88	44.02	44.25	43.83
350	42.31	42.42	43.47	42.80	42.66	42.91	42.82
360	41.18	40.88	40.96	41.15	41.23	41.58	41.60

Background Intensity

Counting Time (sec)	Total Count
106.48	800

TABLE XXI

Low Energy Photon Scattering Intensity from Aluminum Cladding with Uranium Backing

Pulse Height Analyzer - Base Line - 50 volts

Window Width - 2.0 volts

X-ray Unit - 150 Kev, 4 ma. Dynode Voltage - 900 volts

Total Count - 25,600

Cladding Thickness (mils)	Counting Time (sec)				
	Run 1	Run 2	Run 3	Run 4	Run 5
0.0	38.5	38.7	38.5	39.1	37.7
6.7	29.7	29.8	29.4	30.4	30.3
10.0	26.4	27.0	26.7	27.4	28.8
16.7	22.6	23.8	22.6	23.2	24.8
20.5	22.5	21.8	21.0	21.0	21.1
30.9	19.2	19.0	18.6	18.6	18.8
40.9	16.6	16.8	16.9	16.5	16.3
50.9	14.6	14.7	15.2	14.7	14.6
60.9	12.9	13.1	12.7	13.1	12.6
69.3	11.6	12.5	13.7	12.7	12.9

TABLE XXII

Low Energy Photon Scattering Intensity from Stainless Steel Cladding with Uranium Backing

Pulse Height Analyzer - Base Line = 50 volts

Window Width = 2.0 volts

X-ray Unit = 150 Kev, 5 ma. Dynode Voltage = 900 volts

Total Count - 25,600

Cladding Thickness (mils)	Counting Time (sec)				
	Run 1	Run 2	Run 3	Run 4	Run 5
0.0	32.9	34.1	33.9	33.1	34.2
5.0	24.8	24.6	24.8	24.3	24.3
10.0	18.5	19.3	19.8	18.7	19.3
15.0	16.4	15.7	15.8	15.7	16.5
20.0	14.5	13.9	14.2	14.3	14.6
30.0	12.7	12.7	12.2	12.1	12.7
40.0	11.3	11.2	11.6	11.5	11.7
60.0	10.5	10.7	10.6	10.2	10.5
70.0	10.1	9.9	10.3	10.2	10.2

TABLE XXIII

High Energy Photon Scattering Intensity from Zirconium on Uranium Backing

Pulse Height Analyzer - Base Line = 95 volts

Window Width = 9.5 volts

10 mg. Radium Source Dynode Voltage = 900 volts

Total Count - 1,600

Cladding Thickness (mils)	Counting Time (sec)
0.0	40.0
5.0	41.3
10.0	42.7
15.0	43.3
20.0	47.5
25.0	44.5
30.0	44.5
35.0	46.9
40.0	44.0
50.0	46.9

TABLE XXIV

High Energy Photon Scattering Intensity from Stainless Steel on Uranium Backing

Pulse Height Analyzer - Base Line = 95 volts

Window Width = 9.5 volts

10 mg. Radium Source Dynode Voltage = 900 volts

Total Count - 1,600

Cladding Thickness (mils)	Counting Time (sec)
0.0	44.85
5.0	46.48
10.0	47.50
20.0	47.40
30.0	50.04
40.0	49.20
50.0	48.35
60.0	51.60
70.0	49.50

TABLE XXV

High Energy Photon Scattering Intensity from Aluminum on Uranium Backing

Pulse Height Analyzer - Base Line - 95 volts

Window Width - 9.5 volts

10 mg. Radium Source Dynode Voltage - 900 volts

Total Count - 1,600

Cladding Thickness (mils)	Counting Time (sec)
0.0	44.32
7.0	45.20
10.0	46.73
20.0	46.42
30.0	48.42
40.0	52.90
50.4	50.08
60.9	53.85

APPENDIX C

ANALYSIS OF DATA

ANALYSIS OF DATA

L Fluorescence Investigation:

I Aluminum:

For the purpose of determining cladding thickness only the calibrated curve of fluorescent intensity vs. cladding, uncorrected for background and scattering intensities, would be required. For the analysis of the data, however, it was necessary to remove scattering and general room background to obtain the pure fluorescent intensity. Since the scattering intensity from aluminum was only measured at 10 mil intervals it was necessary to interpolate for intermediate values of foil thickness. Interpolation values were taken from Table X.

A. Subtraction of background from scattering intensity:

Thickness (mils)	N_{S+B}	$r^2_{S+B} + r^2_{B}$	$N_{S+B} - B$	$\pm r$
20	119.7	0.0692	114.2	0.263
30	128.5	0.0745	123.0	0.273
40	133.1	0.0800	127.6	0.283
50.4	135.7	0.0800	130.2	0.283
60.9	138.3	0.0857	132.8	0.293

B. Subtraction of background from fluorescent intensity:

Thickness (mils)	N_{F+B}	$r^2_{F+B} + r^2_{B}$	$N_{F+B} - B$	$\pm r$
20	1076.8	5.3376	1071.3	2.34

Thickness (mils)	N_{F+B}	$r^2_{F+B} + r^2_{B}$	$N_{F+B} - B$	$\pm r$
21.8	846.9	3.3136	841.4	1.82
23.6	701.4	2.2516	695.9	1.50
25.4	566.7	1.4896	561.2	1.22
26.7	443.3	0.9041	437.8	0.95
28.5	378.4	0.6577	372.9	0.86
30	302.2	0.4241	296.7	0.65
31.8	269.3	0.3380	263.8	0.58
33.5	238.2	0.2617	232.7	0.51
33.6	239.1	0.2617	233.6	0.51
35.4	215.6	0.2132	210.1	0.46
36.7	191.1	0.1697	185.6	0.41
40	161.6	0.1241	156.1	0.35
43.6	156.1	0.1172	150.6	0.34
45.4	149.6	0.1040	144.1	0.32
50.4	141.7	0.0916	136.2	0.30
60.9	138.9	0.0916	133.4	0.30

C. Subtracting corrected scattering intensity from corrected fluorescent intensity to obtain true fluorescent intensity:

Thickness (mils)	N_F	N_S	$r^2_F + r^2_S$	$N_{F'}$	$\pm r$
20	1071.3	114.2	5.4276	957.1	2.33
21.8	841.4	116.3	3.3136	725.1	1.85
23.6	695.9	118.2	2.3416	577.7	1.53

Thickness (mils)	N_F	N_S	$r_F^2 + r_s^2$	N_F	$\pm r$
25.4	561.2	119.7	1.5796	441.5	1.26
26.7	437.8	120.8	0.9941	317.0	1.00
28.5	372.9	122.1	0.7477	250.8	0.87
30	296.7	123.0	0.5141	173.7	0.72
31.8	263.8	124.1	0.4280	139.7	0.65
33.5	232.7	125.0	0.3517	107.7	0.59
33.6	233.6	125.0	0.3517	108.6	0.59
35.4	210.1	125.9	0.3022	84.2	0.55
36.7	185.6	126.5	0.2597	59.1	0.51
40	156.1	127.6	0.2141	28.5	0.46
43.6	150.6	128.5	0.2072	22.1	0.46
45.4	144.1	128.9	0.1940	15.2	0.44
50.4	136.2	130.2	0.1816	6.0	0.43
60.9	133.4	132.8	0.1816	0.6	0.43

To facilitate analysis of the results the above data was normalized to the initial counting rate. The normalized data for both the raw fluorescent counting rates and fluorescent counting rates with room background and scattering intensities subtracted is tabulated in Tables I and II contained in the section for L Fluorescent Results.

In order to check the experimental results with theory the "Least Squares" method was applied to the data to determine the linear attenuation coefficient of aluminum. In carrying out the computation all error was assumed to lie in μ_i, the linear attenuation coefficient of the i^{th} run. This assumption effectively lumps the unknown, but finite error of the cladding thickness in the attenuation coefficient.

$$\ln I_o - \ln I_{x_i} = \mu_i (X_i - X_o)$$

from the normalized data $\ln I_o = 0$

X_i	$\ln I_{x_i}$	$X_i - X_o$	μ_i	$(X_i - X_o)^2 10^6$	$(X_i \ln I_{x_i}) 10^3$
.02	0	0			
.0218	.277	.0018	154.0	3.24	.50
.0236	.504	.0036	140.0	12.97	1.81
.0254	.774	.0054	143.5	29.16	4.18
.0267	1.107	.0067	165.0	44.89	7.41
.0285	1.340	.0085	157.7	72.25	11.40
.0300	1.704	.0100	170.4	100.00	17.04
.0318	1.925	.0118	163.2	139.10	22.70
.0335	2.180	.0135	161.5	182.00	29.40
.0354	2.430	.0154	157.8	237.00	37.40
				820.6	131.8

$$\mu = \frac{\sum (X_i - X_o) \ln I_{x_i}}{\sum (X_i - X_o)^2}$$

$$\mu = \frac{131.8}{820.6} \times 10^3 = 160.5 \text{ in}^{-1}$$

X_i	ν_i	ν_i^2	X_i	ν_i	ν_i^2
.02	--	--	.0285	2.8	7.85
.0218	6.5	42.25	.0300	9.9	98.00
.0236	20.5	420.00	.0318	2.7	7.29
.0254	17.0	289.00	.0335	1.0	1.00
.0267	4.5	20.20	.0354	2.7	7.29

$$\sum \nu_i^2 = 892.88$$

$$r = 0.6745 \sqrt{\frac{\sum \nu_i^2}{n - q}}$$

$n = i = 9$ $q =$ no. of unknowns $= 1$ $\nu_i = \mu - \mu_i$

$$r = \pm 7.07$$

$$\mu = 160.5 \pm 7.07 \quad (4.4\%)$$

A similar calculation for the fluorescent data uncorrected for background and scattering intensities yielded the following linear attenuation for aluminum:

$$\mu = 125.6 \pm 3.98$$

In order to check the correlation between recorded data and theory the following analysis was performed on the results of the L_{α_1} fluorescent investigation for aluminum:

Uranium L_{III} excitation edge = 0.72216 $\AA$ = 17.17 Kev

L_{α_1} Spectral Line = 0.91053 $\AA$ = 13.62 Kev

Since the maximum energy of the incident X-ray spectrum was 45 Kev it was assumed that the average energy of the excitation photons was equal to the mean excess energy of the incident radiation over the L_{III} excitation edge:

$$\bar{E} = \overline{h\nu} = \frac{45 + 17.17}{2} \text{ Kev} = 31.08 \text{ Kev} \cong 31 \text{ Kev}$$

According to the theoretical value from White: [11]

$$\frac{\mu}{\rho}(31) = 1.01 \text{ cm}^2/\text{gm} \qquad \frac{\mu}{\rho}(13.62) = 10 \text{ cm}^2/\text{gm}$$

$$\rho(\text{Al}) = 2.7 \text{ gm/cm}^3$$

accordingly:

$$\mu_0(31) = 6.93 \text{ in}^{-1} \qquad \mu_0(13.62) = 68.5 \text{ in}^{-1}$$

If we consider the geometry of the fluorescent analysis unit:

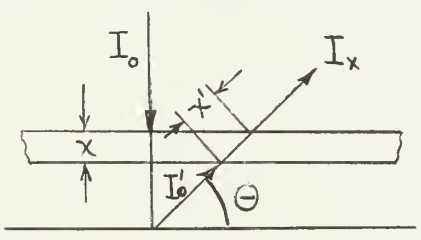

where I_o' is that attenuated portion of the incident radiation which is directed towards the detector. Then it is obvious that:

$$I_o' = kI_o e^{-\mu_o x} = I_1 e^{-\mu_o x}$$

Assuming that there is no attenuation of the uranium fluorescent radiation in the uranium itself:

$$I_x = I'_o e^{-\mu_o' x'} = I'_o e^{-68.5x'} = kI_o e^{-(6.93 + \frac{68.5}{\sin\theta})x}$$

where μ_o is the total attenuation coefficient of the cladding for the incident radiation and μ_o' is the total attenuation coefficient of the cladding for the fluorescent radiation.

$$\mu_{eff} = (6.93 + \frac{68.5}{\sin\theta}) = 160.5 \text{ in.}$$

$$\text{Sin } \theta = \frac{68.5}{153.57} = 0.446$$

$$\theta = 26.5 \text{ degrees}$$

The exact value for the take-off angle was not specified in the equipment manual. Visual measurements gave a take-off angle of approximately 25 degrees. This experimental correlation with theory was considered excellent.

K Fluorescence Investigation

In order to facilitate analysis of the data all fluorescent intensities of the zirconium cladding trials (Table XVIII) were normalized to the mean of the fluorescent intensity obtained with a bare specimen (Table XIX).

The method of "Least Squares" was applied to the fluorescent data to obtain the best fit of the fluorescent attentuation curve vs the zirconium cladding thickness. (See analysis of data for L fluorescent investigation for assumptions) In applying the "Least Squares" method, the attentuation was assumed to be an exponential function over the cladding thicknesses from 0 to 30 mils.

x_i	x_i^2	I_{x_i}	ln I_{x_i}	x_i ln I_{x_i}	μ_i
0	0	1.000			
5	25	0.882	0.1256	0.628	0.0251
5	25	0.914	0.0900	0.450	0.0180
5	25	0.907	0.0980	0.490	0.0196
5	25	0.902	0.1034	0.517	0.0207
5	25	0.882	0.1256	0.628	0.0251
10	100	0.766	0.2670	2.670	0.0267
10	100	0.799	0.2240	2.240	0.0224
10	100	0.810	0.2210	2.210	0.0221
10	100	0.825	0.1921	1.921	0.0192

x_i	x_i^2	I_{x_i}	ln I_{x_i}	x_i ln I_{x_i}	μ_i
10	100	0.794	0.2300	2.300	0.0230
15	225	0.739	0.3030	4.545	0.0202
15	225	0.726	0.3210	4.815	0.0214
15	225	0.746	0.2940	4.410	0.0196
15	225*	0.772	0.2590	3.885	0.0173
15	225	0.752	0.2850	4.275	0.0190
20	400	0.698	0.360	7.200	0.0180
20	400	0.629	0.464	9.280	0.0232
20	400	0.682	0.385	7.700	0.0193
20	400	0.652	0.429	8.580	0.0215
20	400	0.695	0.364	7.280	0.0182
25	625	0.588	0.531	13.275	0.0212
25	625	0.593	0.522	13.050	0.0209
25	625	0.603	0.508	12.700	0.0203
25	625	0.611	0.493	12.325	0.0197
25	625	0.591	0.528	13.200	0.0211
30	900	0.502	0.689	20.670	0.0230
30	900	0.516	0.663	19.890	0.0231
30	900	0.539	0.619	18.570	0.0206
30	900	0.520	0.655	19.650	0.0218
30	900	0.506	0.681	20.430	0.0254

$\sum x_i^2 = 11,375$ $\sum x_i \ln I_{x_i} = 243.784$

$$\mu = \sum \frac{x_i \ln I_{xi}}{x_i^2} = 21.4 \text{ in}^{-1}$$

x_i	μ_i	$\nu_i \times 10^4$	$\nu_i^2 \times 10^8$
5	0.0251	37	1369
5	0.0180	34	1126
5	0.0196	18	324
5	0.0207	7	49
5	0.0251	37	1369
10	0.0267	53	2809
10	0.0224	10	100
10	0.0221	7	49
10	0.0192	22	484
10	0.0230	16	256
15	0.0202	12	144
15	0.0214	0	0
15	0.0196	18	324
15	0.0173	41	1681
15	0.0190	24	576
20	0.0180	34	1126
20	0.0232	18	324
20	0.0193	21	441
20	0.0215	1	1
20	0.0182	32	1024

x_i	μ_i	$\nu_i \times 10^4$	$\nu_i^2 \times 10^8$
25	0.0212	2	4
25	0.0209	5	25
25	0.0203	11	121
25	0.0197	17	289
25	0.0211	3	9
30	0.0230	16	256
30	0.0231	17	289
30	0.0206	8	64
30	0.0218	4	16
30	0.0254	40	1600

$$\sum \nu_i^2 = 16{,}249 \times 10^8$$

$$r = 0.6745 \sqrt{\frac{\sum \nu_i^2}{n - q}}$$

$n = 30$ $\qquad$ $q = 1$

$$r = \pm 1.59$$

$$\mu = 21.4 \pm 1.6 \quad (7.4\ \%)$$

II Tubular Fuel Element - Zircalloy II Cladding:

A series of tubular specimens with various known cladding thicknesses was not available. The particular specimen to be tested (see Fig. III) had been visually measured at one end by Nuclear Metals Inc., and a plot of cladding thickness vs. angular orientation was available.

To correlate the fluorescent readings taken using the uranium K series (Table XX) it was necessary to make the following assumptions:

1. The attenuation coefficient of Zircalloy II is identical to that of zirconium.
2. The tubular specimen was assumed to be flat (a reasonable approximation for the geometry used)
3. The maximum intensity of fluorescent radiation corresponded to the minimum cladding thickness as shown by the data of Nuclear Metals Inc.

Using the above assumptions, and a correction for differences in angular orientation between the tubular element and the flat slab approximation, an effective linear attenuation coefficient for the tubular element could be derived:

where x' is the effective path length of the photon in the cladding material.

For the flat slab approximation:

$$x' = \frac{2\,t}{\cos 45} \qquad \text{(see Fig. XX)}$$

For the tubular element:

$$x' = t\left[\frac{1}{\sin 28.2} + \frac{1}{\cos 28.2}\right] \quad \text{(see Fig XXI)}$$

Therefore, for the tubular fuel element:

$$\mu_e = 24.6 \text{ in}^{-1}$$

Using this effective attenuation coefficient a plot of normalized intensity vs. cladding thickness is:

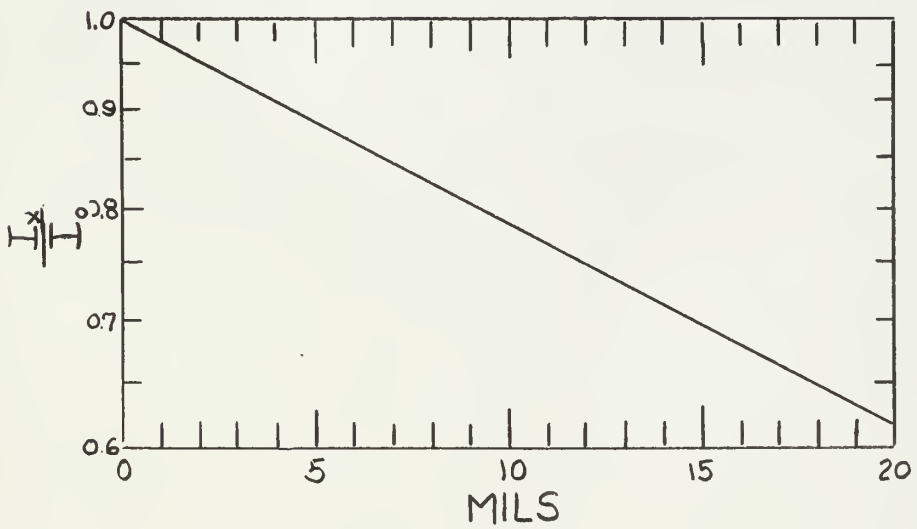

Figure XXIII Intensity of Uranium K Series Fluorescent Radiation vs. Zircalloy II Cladding Thickness

The maximum fluorescent intensity recorded is assumed to correspond to the minimum cladding thickness of the specimen. The theoretical bare uranium fluorescent intensity can be found as follows:

The minimum cladding thickness indicated by the data of Nuclear Metals, Inc., was 5 mils, while the maximum intensity recorded in the data was 672 CPS. From Figure XXIII the normalized intensity for 5 mils of cladding is 0.885. The theoretical intensity for bare uranium can then be found from the relationship:

$$\frac{I_x}{I_o} = \text{normalized intensity at } x$$

$$I_o = 760 \text{ CPS}$$

All fluorescent readings were normalized to the theoretical I_o and a corresponding cladding thickness was determined from Figure XXIII. The results of these calculations are tabulated below:

TABLE XXVI

Angular Orientation vs. Cladding Thickness

Tubular Fuel Element

θ	Cladding Thickness (mils)
0	8.4
10	6.5
20	9.0
30	11.5
40	9.0
50	5.6
60	6.5
70	9.4
80	8.4
90	6.6
100	5.4
110	7.0
120	10.4
130	10.9
140	7.8
150	8.6
160	12.0
170	9.7

θ	Cladding Thickness (mils)
180	6.6
190	5.9
200	4.6
210	11.1
220	9.7
230	5.6
240	6.3
250	7.8
260	9.4
270	8.0
280	5.0
290	5.0
300	8.6
310	10.0
320	6.6
330	6.6
340	11.1
350	9.9

III Analysis of the data for K fluorescent intensity as a function of thickness of stainless steel cladding (Table XVII) indicated no consistent significant changes in intensity of fluorescent radiation for changes in cladding thickness.

Cladding Thickness (mils)	CPS	$\pm\sigma$
0.0	2034	13
5.0	1932	12
10.0	2034	13
20.0	1961	12
30.0	2088	13
40.0	2076	13
50.0	2038	13
60.0	2086	13

Low Energy Photon Scattering Investigation:

In order to check correlation of the results of the photon scattering investigation with theory the following relationship was developed and applied to the data for low energy photon scattering by aluminum cladding:

The probability that a scattering event occurs while a photon is traversing a thickness x of the cladding material is given by:

$$P_{SCAT} = (1 - e^{-\sigma_s x})$$

where σ_s is the scattering coefficient of the cladding material at the energy of the incident photon. The intensity of radiation scattered through an angle of 90 degrees to the incident beam can be expressed by:

$$I_{90} \propto I_o(1 - e^{-\sigma_s x})$$

or:

$$I_{90} = k\,(1 - e^{-\sigma_s x})$$

This scattered radiation has a finite probability of interacting with the cladding material before escaping from the surface. If the scattered photons are assumed to be uniformly produced throughout the foil (good only for very thin foils) the mean probability of photons escaping can be approximated by:

$$\frac{(1 + e^{-\mu_o' x})}{2}$$

where μ_o' is the total attenuation coefficient of the cladding material for the energy of photons scattered through 90 degrees. The intensity of radiation at 90 degrees to the incident beam can then be approximated by:

$$I_{90} = k\ (1 - e^{-\sigma_c x})(1 + e^{-\mu_o' x})$$

In the cladding problem the initial intensity is not zero since the uranium will contribute an initial intensity, I_b, which will be attenuated by the cladding as:

$$I_{bx} = I_{bo}\ e^{-(\mu_o + \mu_o')x}$$

where μ_o and μ_o' have the meanings previously assigned. The normalized scattering intensity from a clad uranium surface can then be approximated by the relationship:

$$I_{NOR} = k\ (1 - e^{-\sigma_s x})(1 + e^{-\mu_o' x}) + e^{-(\mu_o + \mu_o')x} \qquad (18)$$

It should be noted that x is the effective thickness of cladding presented to the incident X-ray beam, and is therefore a function of the geometry of the experiment.

Correlation of equation (18) with the experimental data was checked as follows:

By assuming a linear variation of the pulse height analyzer base line with photon energy the energy of the scattered photon was determined to be 70 Kev. The energy of the incident photon required to produce a 70 Kev photon after scattering through 90 degrees can be obtained by employing equation (7).

$$\frac{1}{h\nu'} - \frac{1}{h\nu_o} = \frac{1}{m_o c^2} (1 - \cos \theta)$$

$$h\nu_o = 81 \text{ Kev}$$

The following values were obtained from tabulated values for the attenuation coefficients of aluminum:

81 Kev: $\mu_o = 1.233$ in $\quad \sigma_s = 0.891$ in

70 Kev: $\mu_o' = 1.408$ in

Since the specimen was oriented at 45 degrees to the incident beam the effective thickness, x, is given by:

$$x = 1.414\ t$$

where t is the thickness of cladding material on the uranium fuel element.

By substituting the above constants in equation (18) and using the experimentally determined value of normalized intensity for 30 mils of aluminum cladding, an empirical value for the constant, k, was determined. Values of

normalized intensity for 10, 20, 40 and 70 mils of aluminum cladding thickness were then calculated. The results of these calculations, and the corresponding, experimentally determined values are tabulated below:

Cladding Thickness (mils)	Itheor.	Iexp.
0.0	1.00	1.00
10.0	1.36	1.40
20.0	1.69	1.75
30.0	2.02	2.02
40.0	2.34	2.31
70.0	3.23	3.01

Considering the assumptions made in the development of equation (18), and in selecting values of the attenuation coefficients, the correlation is considered good.

High Energy Photon Scattering:

For the analysis of data it was necessary to remove the overall room background to determine the change in scattered intensity as a function of cladding thickness.

An analysis of the scattering data is presented below for the cladding materials of aluminum, 304 stainless steel and zirconium.

Aluminum Cladding

Thickness (mils)	N_{S+B}	$r^2_{S+B} - r^2_{B}$	$N_{S+B} - B$	$\pm r$
0.0	36.10	1.12	13.86	1.06
7.0	35.45	1.10	13.21	1.05
10.0	34.25	1.05	12.01	1.02
20.0	34.50	1.05	12.26	1.02
30.0	33.10	1.00	10.86	1.00
40.0	30.28	0.89	8.04	0.94
50.4	31.95	0.95	9.71	0.97
60.9	29.76	0.86	7.52	0.93

304 Stainless Steel

Thickness (mils)	N_{S+B}	$r^2_{S+B} + r^2$	$N_{S+B} - B$	$\pm r$
0.0	35.76	1.21	13.52	1.11
5.0	33.60	1.01	11.36	1.00
10.0	33.70	1.01	11.46	1.00
20.0	33.80	1.03	11.56	1.02
30.0	31.79	0.94	9.55	0.97
40.0	32.56	0.97	10.32	0.99
50.0	33.14	1.00	10.90	1.00
60.0	31.00	0.92	8.76	0.95
70.0	32.32	0.97	10.08	0.99

Zirconium:

Thickness (mils)	N	$r^2_{S+B} + r^2_B$	$N_{S+B} - B$	$\pm r$
0.0	40.00	1.31	17.76	1.14
5.0	38.70	1.18	16.46	1.09
10.0	37.44	1.14	15.20	1.07
15.0	36.90	1.16	14.66	1.08
20.0	33.66	1.02	11.42	1.01
25.0	35.91	1.12	13.67	1.06
30.0	35.91	1.12	13.67	1.06
35.0	34.10	1.03	11.86	1.02
40.0	34.36	1.14	14.12	1.07
50.0	34.10	1.03	11.86	1.02

It is obvious in analyzing the above data for each cladding material that consistent significant changes in scattering intensity for changes of cladding thickness do not exist.

LIST OF REFERENCES

1. L.S. Birks, E.J. Brooks and H. Friedman, "Fluorescent X-ray Spectroscopy", Analytical Chemistry, vol. 25, (1953), pp 668 - 748.

2. A. H. Compton, Physical Review, vol. 21, p 715; vol. 22, p 409, (1923).

3. B. D. Cullity, Elements of X-ray Diffraction, Addison Wesley Publishing Co., Inc., Reading, Mass. (1956) pp 402 - 422.

4. C. M. Davidsson and R.D. Evans, Revs. Modern Physics, vol. 24 (1952), p 79.

5. R. D. Evans, The Atomic Nucleus, McGraw - Hill Book Co., New York, (1955).

6. O. Klein and Y. Neshina, Z. Physik, vol. 52, (1928), p 853.

7. W. J. McGonnagle, " Nondestructive Testing of Reactor Components", Nucleonics, vol. 15, no. 10, (1957), p 78

8. A. T. Nelms, " Graphs of the Compton Energy-Angle Relationship and the Klein-Neshina Formula from 10 Kev to 500 Mev", Natl. Bu. of Stds. (US), Circ. 542, (1953)

9. F. K. Richtmyer, E. H. Kennard and T. Lauritsen, Introduction to Modern Physics, McGraw Hill Book Co., Inc., New York, (1955)

10. J. J. Thomson, The Corpuscular Theory of Matter, Constable and Company, Ltd., London, (1907)

11. G. R. White, " X-ray Attenuation Coefficients from 10 Kev to 100 Mev, Natl. Bu. of Stds. (US), Report no. 1003, (1952).

12. " An Instrument for Measuring the Thickness of Materials by Gamma Rays", Journal of Scientific Instruments, vol. 23, (1946), p 133.